Large Igneous Province sulfur emissions have long-term (>1000 years) effects on the ocean carbon cycle

Hee Jun Cheong[1], Tushar Mittal[2]*, Courtney Jean Sprain[1], Isabel M Fendley[2]

[1]University of Florida, Department of Geological Sciences, Gainesville, FL 32611

[2]Pennsylvania State University, Department of Geosciences, University Park, PA 16802

Corresponding author: Tushar Mittal (tmittal@psu.edu)

Key Points:

- Volcanic CO_2 and SO_2 emissions have complex and interconnected effects on the ocean-atmosphere system and biosphere
- Results show sulfate aerosol driven cooling has long-lasting (>1000 years) effects on the ocean carbon cycle
- Conventional assumption of strict timescale separation between the effects of volcanic CO_2 and SO_2 emissions is incorrect

Abstract

Large Igneous Province (LIP) eruptions are thought to have driven environmental and climate change over wide temporal scales ranging from a few to thousands of years. Since the radiative effects and atmospheric lifetime of carbon dioxide (CO_2, warming) and sulfur dioxide (SO_2, cooling) are very different, the conventional assumption has been to analyze the effects of CO_2 and SO_2 emissions separately and add them together afterward. In this study, we test this assumption by analyzing the joint effect of CO_2 and SO_2 on the marine carbonate cycle using a biogeochemical carbon cycle box model (LOSCAR). By performing model runs with very fine temporal resolution (~0.1-year timestep), we analyze the effects of LIP carbon and sulfur gas emissions on timescales ranging from an individual eruption (hundreds to thousands of years) to the entire long-term carbon cycle (>100,000 years). We find that, contrary to previous work, sulfur emissions have significant long-term (>1000 years) effects on the marine carbon cycle (dissolved inorganic carbon, pH, alkalinity, and carbonate compensation depth). This is due to two processes: the strongly temperature-dependent equilibrium coefficients for marine carbonate chemistry and the few thousand-year timescale for ocean overturning circulation. Thus, the effects of volcanic sulfur are not simply additive to the impact of carbon emissions. We develop a causal mechanistic framework to visualize the feedbacks associated with combined carbon and sulfur emissions and the associated timescales. Our results provide a new perspective for understanding the complex feedback mechanisms controlling the environmental effects of large volcanic eruptions over Earth history.

Plain Language Summary

Large Igneous Province (LIP) eruptions are among the largest volcanic events in Earth history and have been linked with environmental catastrophes such as mass extinctions and oceanic anoxic events. One of the main ways these volcanic events affect the environment is through the emission of climate-active gases, primarily carbon dioxide (CO_2) and sulfur dioxide (SO_2). These gases are often thought of as behaving independently, as CO_2 causes long-term climate warming while SO_2, which turns into sulfate aerosols, causes short-term climate cooling. However, in addition to directly causing climate change, both gases also cause more complex environmental changes, including changes to the ocean carbon cycle (e.g., ocean

acidification and the amount and chemical species of dissolved carbon). Our study uses a long-term marine carbon cycle box model to investigate these complex effects. We find that the assumption that the effects of each type of gas are independent is not accurate. Instead, we show that the carbon-cycle effects of sulfur emissions, in particular, can persist on long timescales (>1000 years) in addition to short-term cooling. Our results provide a new perspective for understanding the environmental effects of large volcanic eruptions over Earth history.

1. Introduction

Volcanism is a key driver of change in ecosystems and the ocean-atmosphere system on Earth. Volcanic eruptions can strongly perturb the climate and biosphere on a wide range of temporal scales: from years to decades for a single large volcanic eruption to millions of years for the emplacement of a Large Igneous Province (LIP; e.g., the Siberian Traps). Short-term environmental effects of single large eruptive events have been directly observed (e.g., the Pinatubo 1991 eruption, Self et al., 1993; Fay et al., 2023) and are reasonably well understood. Longer-term environmental effects that are difficult to observe on human timescales are more challenging to understand and require disentangling a complex set of Earth system feedbacks (Black et al., 2021; Mather and Schmidt, 2021). These complex direct and indirect Earth system feedbacks, which occur over a range of timescales (Figure 1), are particularly critical for understanding how volcanic eruptions associated with LIP emplacement affected the ocean-atmosphere system and the biosphere on geological timescales (>1000 years).

LIPs constitute some of the largest volcanic events in Earth's history representing millions of km^3 of predominantly basaltic lavas with individual eruptions having erupted volumes ~1000s km^3 (Wignall, 2001; Courtillot, 2002; White et al., 2005; Ernst, 2014; Kasbohm et al., 2021). Multiple paleoclimate and geochronological studies have shown that the emplacement of LIPs occurred simultaneously (within order 10,000 year uncertainty) with severe environmental crises such as mass extinctions and oceanic anoxic events (Courtillot and Renne, 2003; Clapham and Renne, 2019; Kasbhom et al., 2021). However, the emplacement of LIPs does not always lead to the same type or magnitude of environmental response. Understanding which factors control different Earth system responses remains one of the key challenges in understanding how volcanism affects climate over Earth history. To elucidate the causal

relationship between LIPs and environmental crises, and generally the long-term effects of large-scale volcanism on the Earth system, it is thus important to understand how these volcanic events mechanistically affected the environment beyond simple temporal correlation.

Volcanic eruptions associated with LIPs, as well as other large volcanic events, are hypothesized to influence the global ocean-atmosphere system through the rapid atmospheric emission of large amounts of climatically active volcanic gases (e.g., SO_2, CO_2, H_2O, halogens). Specifically, carbon dioxide (CO_2) and sulfur dioxide (SO_2), sourced either from direct degassing of LIP lavas (and magma) or from the heating of carbon- and sulfur-rich sediments by volcanic intrusives, are the two main gases linked to perturbations of the ocean-atmosphere system (See Figure 1a, Clapham and Renne, 2019; Mather and Schmidt, 2021; Callegaro et al., 2023).

Classically, the environmental effects of these two volcanic gases have been analyzed separately, because of the assumption that each influences the environment on different timescales. Volcanic CO_2 is a greenhouse gas and has a long residence in the ocean-atmosphere system (hundreds of years in the atmosphere, and hundreds of kiloyears in the marine carbon cycle). Consequently, the release of CO_2 generally results in long-term (10–100+ kiloyears) environmental impacts (e.g., greenhouse warming, changes in weathering) (Figure 1b). In contrast, if volcanic SO_2 reaches the stratosphere, it can oxidize to form sulfate aerosols over the timescale of a few months and result in global cooling for a few years before being deposited on land/oceans (Robock, 2000; Wignall, 2001; Delmelle, 2003). Given the relatively short atmospheric residence times (months to years), volcanic sulfur will only result in short-term direct environmental impacts (e.g., cooling and acid rain) (Wignall, 2001, Figure 1b) unless continuously erupted. Thus, it is often assumed that volcanic SO_2 emissions are not relevant to directly understanding the long-term effects of volcanic eruptions, particularly in the case of LIP-associated eruptions. Within this perspective, the impact of large eruptions can be conceptualized, to first order, as a combination of short-term cooling (up to a few years post the eruption from SO_2 emissions) and long-term warming (from CO_2 emissions).

However, this timescale separation assumption may not be fully correct when accounting for the indirect effects of volcanic carbon and sulfur on the Earth system, modulated principally through the marine carbon cycle (Figure 1a). For instance, sulfate has a long residence time in the oceans, and thus volcanism can affect ocean pH and alkalinity through direct sulfate

deposition from the atmosphere. Even more importantly, stratospheric sulfate-associated cooling can lead to significant changes in marine carbonate equilibrium chemistry since the equilibrium partition coefficients in marine carbonate chemistry (Eqn. 1) with carbonic acid (H_2CO_3), bicarbonate (HCO_3^-), and carbonate ions (CO_3^{2-}) are strongly temperature dependent (See Section 2.2, Figure 2). The consequent changes in pH and atmospheric pCO_2 in turn may affect ocean carbonate dissolution/carbonate burial and thus the long-term marine carbon cycle response to large volcanic eruptions.

$$CO_2(atm) \rightleftharpoons CO_2(aq) + H_2O(l) \rightleftharpoons H^+ + HCO_3^- \rightleftharpoons CO_3^{2-} + 2H^+ \qquad \text{(Eqn. 1)}$$

The assumption of timescale separation has strongly influenced existing work on understanding the effects of LIP eruptions and has directly motivated two distinct modeling approaches for understanding their environmental impacts:

One approach uses complex, high spatial resolution, global climate models (e.g., GLOMAP in Schmidt et al., 2016; CESM1 in Black et al., 2018; CLIMBER-3α+C in Landwehrs et al., 2020; Goddard Earth Observing System Chemistry-Climate Model in Guzewich et al., 2022) that are developed to analyze interactions within the Earth system (i.e., atmosphere, ocean, land, etc.) on short timescales (years to 10,000 years at most). Typically, the focus of these studies is the atmospheric radiative effects due to aerosols and the consequential changes in surface temperature and global ocean overturning circulation. For computational reasons, these models are primarily physical models with limited ocean biogeochemistry and can thus only capture the short-term carbon cycle response. Black et al. (2018) modeled the effects of carbon and sulfur with atmospheric circulation using 3D climate modeling (CESM1), including atmospheric, ocean dynamics, and aerosol models. Their results help highlight the atmospheric responses from released carbon and sulfur by demonstrating temperature changes and circulation for the ocean parameters from the associated short-term cooling and long-term warming. However, due to the absence of a biogeochemical cycling model, there are limitations in evaluating ocean geochemistry and carbon cycle responses from both carbon and sulfur jointly. The other approach uses geochemical box models/intermediate complexity Earth system models that utilize simplified ocean-atmospheric dynamics and ocean biogeochemistry to assess the long-term (10,000 years and longer) carbon cycle responses to eruptions. Multiple studies have used these types of models to simulate the long-term carbon cycle response for a number of

different LIPs (e.g., LOSCAR in Zeebe, 2012; Landwehrs et al., 2020; Hull et al., 2020; Cox and Keller, 2023; Black et al. 2024). However, the focus of these studies is typically on volcanic CO_2 emissions as the climate driver. In the few studies that incorporate the combined effects of carbon and sulfur emissions together on the long-term carbon cycle (Hull et al., 2020; Cox and Keller, 2023), significant simplifications with regard to the volcanic forcing timescale are made. For instance, in Cox and Keller (2023), a few thousand-year model timestep is used for computational reasons to do parameter inversions. In Hull et al. (2020), only some of the potential carbon and sulfur associated processes are included - the effect of volcanically sourced sulfate aerosols on ocean alkalinity, and not temperature. More recently, Cox and Keller (2023) have incorporated these missing components in the LOSCAR model and used it for Bayesian eruption history inversion. However, for computational reasons, the model timestep in their study is ~ 5000 yrs. A variety of volcanological, paleomagnetic, and geochronological evidence (Mittal et al., 2021; Self et al., 2022; Rader et al., 2024) suggest that the individual LIP eruptions lasted for a few years to hundreds of years at most with significant time breaks (>1000–10,000 yr), instead of long continuous eruptions for a few thousand years as assumed in these studies. Thus, it is unclear if their modeled effects from the same total volume of sulfur emissions, but spread over much longer timescales with lower amplitude, would give the same response as a more realistic eruption scenario.

Furthermore, the focus of some of these studies has been on analyzing the integrated feedback between the ocean-atmosphere cycle and biological organisms to compare model results to specific observational datasets (Landwehrs et al., 2020; Hull et al., 2020; Cox and Keller, 2023). For instance, Landwehrs et al. (2020) integrated both a climate model (CLIMBER-3α+C Earth System model) and a geochemical box model (LOSCAR, Zeebe (2012)) with carbon and sulfur emissions to model end-Triassic volcanism associated with the Central Atlantic Magmatic Province. Analogously, Le Hir et al. (2020) used a climate-carbon-biodiversity coupled model (ECO-GEOCLIM) to assess the impact of the Chicxulub impact and volcanic activity (Deccan Traps) on the productivity and diversity of marine organisms. However, given the complexity of the model and the focus on data-proxy data comparison, it is very challenging to understand how volcanic carbon and sulfur jointly affect the carbon cycle from a mechanistic perspective, especially the different feedback loops in the marine carbon cycle system.

Thus, there is a clear knowledge gap in the existing work on the combined effects of carbon and sulfur release over relevant timescales (sub-yr to 100s kyr). To untangle the impact of different Earth system processes (Figure 1), we need to understand, in a process-based framework, the causal relationship between the release of volcanic carbon and sulfur and their impacts on different environmental tracers (pH, temperature, alkalinity, carbonate compensation depth).

In this study, we use a biogeochemical box model to test the hypothesis that volcanic sulfur can have a significant long-term effect on the marine carbon cycle (pH, alkalinity, and carbonate compensation depth) and that the effects of volcanic sulfur are not simply additive to the impact of volcanic carbon alone. If correct, our hypothesis suggests that to analyze the effects of large eruptions, particularly LIP eruptions, we must consider the carbon and sulfur volcanic emissions jointly (in contrast to most existing work). Additionally, we develop a causal mechanistic framework to understand the effects of combined carbon and sulfur emissions with an emphasis on determining the feedback amplitudes and characteristic timescales. This analysis will help determine what time resolution is required in climate models to capture the feedbacks correctly. For simplicity, we focus exclusively on the ocean geochemical carbon cycle - a major driver of global environmental change and the control on most paleoclimate records. While LIP eruptions likely significantly impact atmospheric chemistry and dynamics, ocean circulation, and terrestrial systems, isolating the inorganic marine carbon cycle allows us to develop a careful process-based understanding, which can then be subsequently expanded to incorporate other Earth system components.

For our analysis, we use a multi-box earth system model, LOSCAR (Long-term Ocean-atmosphere-Sediment CArbon cycle Reservoir Model; Zeebe, 2012), modified to incorporate the effects of sulfate aerosol-driven cooling and the effect of sulfur on ocean alkalinity. We vary eruption parameters such as the total amount of carbon and sulfur released and the timescale over which the gases are released (hypothesized to scale to volatile release from erupted lava and eruption duration, respectively) across a large parameter space. By performing model runs with very fine temporal resolution (~0.1 year timestep), we can analyze the effects of carbon and sulfur release on timescales ranging from individual volcanic eruptions (hundreds to thousands of years) to the entire long-term carbon cycle (>100,000 years, Figure 1b). We focus on continental flood basalt (CFB, i.e. LIPs that erupted through continental crust) eruptions for this

work since they are the best examples of volcano-climate-ecosystem interaction due to their large amplitude and associated environmental change based on paleoclimate proxies (Clapham and Renne 2019). To focus on the impact of eruptive gas release on the marine carbon cycle, we keep the ocean circulation and biological productivity parameters the same pre- and post-eruption. Our choice is also motivated in part by the fact that previous studies (Black et al., 2018, Schmidt et al., 2016) have already analyzed the “physical” effect (ocean and atmospheric dynamics) of carbon and sulfur volcanic emissions, but not the "geochemical" carbon cycle effects (changes in marine carbon cycle). To elucidate the role of the simultaneous release of carbon and sulfur, we perform two types of model runs, one carbon-only with the original LOSCAR setup (see supplementary text S1), and one combined carbon and sulfur using our modified LOSCAR setup (including cooling and changes in alkalinity from volcanic sulfur; section 3.1).

We focus on modeling the effects of a single LIP eruption (i.e., a single lava flow-field, or gas emission event) as a source of CO_2 and sulfate into the atmosphere (e.g., Self et al., 2022). In reality, LIPs have multiple (hundreds) eruptions as part of a long million-year scale eruption history. However, realistic eruption histories make it difficult to disentangle causal relationships without first understanding the effects of a single eruption, as the volatile gas release volume and eruption duration are varied. We also do not attempt a direct comparison with paleoclimate records here. A model-data comparison would require incorporation of both a multiple eruption history over a million years (but with <1 year time resolution to resolve the individual eruption effects) as well as the physical (ocean dynamics) impacts of the eruptions on the atmosphere-ocean system – this is beyond the scope of the current work.

In the following sections, we start with a theoretical background of the main marine carbon environmental tracers and how volcanism could affect them. This analysis is used to develop a conceptual causal diagram with various feedback loops (Section 2). Next, we describe the modeling framework and our model parameters (Section 3), followed by the model results (Section 4). We use these results to update the causal diagram with various feedback loops and associated timescales for the release of carbon and sulfur and the resulting environmental effects. We close with a discussion of the implications of our results in the context of LIP eruptions as well as coupling with physical feedbacks (e.g., changes in ocean circulation) that are not included in our model (Section 5).

2. Theoretical Background

2.1. Primary Environmental Tracers of Interest

In our analysis, we will focus primarily on five marine environmental tracers: temperature, pH, total alkalinity (TA), dissolved inorganic carbon (DIC), and the carbonate compensation depth (CCD). These tracers were chosen because they have a significant influence on marine ecosystems and characterize the state of the marine carbonate system following perturbations, for example, volcanic eruptions (e.g., Hull et al., 2020; Landwehrs et al., 2020; Le Hir et al., 2020; Mather and Schmidt, 2021).

DIC (mmol kg^{-1}) refers to the sum of the concentration of all dissolved inorganic carbon compounds, including dissolved CO_2, carbonic acid (H_2CO_3), bicarbonate (HCO_3^-), and carbonate ions (CO_3^{2-}) (see Eqn. 1). pH is the negative logarithm of proton concentration: -log $[H^+]$ and is thus a key variable in the marine carbonate system.

Ocean alkalinity refers to the capacity of seawater to neutralize acids and, hence buffer changes in pH. Titration (or total) alkalinity (TA) refers to the excess of proton acceptors over proton donors. From here, TA and alkalinity (in mmol kg-1) will be used interchangeably in the rest of the text. When considering the CO_2 – H_2O system and a few other acid–base systems such as sulfate, borate, phosphate, and ammonia, TA can be defined (also following the LOSCAR model – Zeebe, 2012) as Middleburg et al. (2020):

$$TA = HCO_3^- + 2CO_3^{2-} + B(OH)_4^- + HPO_4^{2-} + 2PO_4^{3-} + NH_3 + HS^- + 2S^{2-} + OH^- - H^+ - HSO_4^- - 2SO_4^{2-} \quad \text{(Eqn. 2)}$$

Given the large relative concentrations of $[CO_3^{2-}]$ and $[HCO_3^-]$ at neutral pH compared to H+ and small changes in other acid–base species, besides sulfate (from volcanic sulfur) during our model simulations, TA can be simplified as follows (Middleburg et al., 2020; Tosca and Tutolo, 2023):

$$TA \cong 2[CO_3^{2-}] + [HCO_3^-] - 2SO_4^{2-} \quad \text{(Eqn. 3)}$$

Overall, TA is a metric for the ocean's ability to precipitate carbonate and buffer against pH variations. This neutralizing ability plays a significant role in maintaining marine chemical balance and supporting marine life, especially calcifying organisms such as corals and mollusks, which rely on stable pH levels to build and sustain their calcium carbonate structures. Because of the interdependence between these environmental tracers (Eqn. 1), the marine carbonate system

(concentration of each DIC species) is uniquely defined by a combination of any two tracers among TA, pH, DIC, and pCO_2 (units of μatm).

The last environmental tracer of interest for our analysis is the CCD - the depth at which calcium carbonate ($CaCO_3$) supply from ocean productivity and water column/seafloor dissolution are balanced (Eqn. 4, Wood et al., 2022).

$$CaCO_3 + CO_2 + H_2O \rightleftharpoons Ca^{2+} + 2HCO_3^- \quad \text{(Eqn. 4)}$$

Below this depth, the solubility of $CaCO_3$ increases due to higher pressure and lower temperatures, causing any $CaCO_3$ materials to dissolve more quickly than they can accumulate. Hence, no $CaCO_3$ is preserved on the seafloor. $CaCO_3$ precipitation and dissolution are critical components of the marine carbon cycle since the dissolution leads to a two-unit increase in TA and a one-unit increase in DIC. In contrast, the opposite is the case for the precipitation (see Figure 2a and b). Thus, changes in CCD act as a critical part of the Earth system response to perturbations in the atmospheric pCO_2 and marine carbonate chemistry following volcanic eruptions.

2.2 Anticipated Effects of Volcanic CO_2 and SO_2 emissions:

Based on the theoretical understanding of the marine carbon cycle and prior work on volcanic forcings, we here provide a brief overview of how volcanic CO_2 and SO_2 emissions may influence ocean pH, temperature, alkalinity, and CCD. This forms the basis for our causal diagram (Figure 3), which describes the various feedbacks associated with the CO_2 and SO_2 emissions. The causal diagram in turn provides a reference framework to interpret our model results in subsequent sections.

Firstly, both gases affect the temperature in the atmosphere: volcanic CO_2 increases pCO_2, which drives warming due to the greenhouse effect (Romps et al., 2022). In contrast, SO_2 emissions, if they reach the stratosphere, oxidize to form sulfate aerosols over a few months timescale and can lead to cooling due to increased shortwave scattering by aerosols (Robock, 2000; Wignall, 2001; Delmelle, 2003). Next, these changes in atmospheric temperature will affect the ocean: the surface ocean responds quickly to atmospheric temperature; however, it takes longer to diffuse heat into the deeper ocean with timescales ranging from years to 1000s of years, depending on global ocean overturning circulation rates and spatial patterns (Gupta and Marshall, 2018). Importantly, changes in ocean temperature strongly affect (i) the solubility of

various geochemical species in seawater; for example, the solubility of gaseous O_2 decreases with increasing temperature, making a warmer ocean less oxygenated and (ii) the equilibrium coefficients for the reactions in marine carbonate chemistry (Eqn. 1); for example, changes in seawater temperature at constant DIC and TA lead to strong changes in equilibrium atmospheric pCO_2 and ocean pH (Figure 2c and 2d).

To illustrate these dependencies, we use pyCO2SYS (Xu et al., 2017; Humphreys et al., 2022); to calculate the equilibrium ocean carbonate chemistry for a range of TA-DIC-seawater temperature conditions for both the shallow and deep ocean. In Figure 2c and d, we show how the equilibrium pCO_2 and pH change as a function of both TA and temperature (at a constant DIC of 2 mmol/kg). As expected, at higher TA, the equilibrium atmospheric pCO_2 decreases, and the pH increases. However, seawater temperature strongly affects the exact value of both these tracers – increasing temperature from 5 to 35°C can lead to up to a 4000 ppm pCO_2 increase and 0.4 unit pH decrease. Moreover, the amplitude of the change is dependent on both the value of TA and DIC, while seawater pressure (i.e., depth) has a small impact on pH changes only (See Supplementary Dataset S1). Thus, we expect that ocean temperature changes due to volcanic carbon and sulfur emissions will have a significant but complex impact on the primary environmental tracers (described in the previous section) as temperature evolves in the atmosphere and different parts of the ocean over different timescales.

To visualize the various non-intuitive feedbacks and isolate the dominant effects and the associated timescales, we generate a causal diagram to illustrate step-by-step how volcanic gases affect the ocean-atmosphere system (Figure 3). The causal diagram has two causal sequences for CO_2 and SO_2, respectively. Both start with temperature changes and are followed by interlinked changes in marine chemistry, atmospheric pCO_2, and temperature on various timescales. Although we made the causal diagram structure based principally on a theoretical understanding of marine carbonate chemistry, the reaction rates/associated timescales are unclear and require our LOSCAR model results for quantitative estimates.

Considering volcanic CO_2 emissions, rising atmospheric pCO_2 leads to increased CO_2 absorption by the oceans (changes in both DIC and TA), resulting in ocean acidification (decrease in pH) since the ocean is a key surface carbon reservoir. For instance, about half of the anthropogenic carbon emissions are presently stored in the shallow ocean (Gattuso et al. 2015).

This acidification promotes the dissolution of calcium carbonate into calcium and bicarbonate ions (Eqn. 1), thereby shallowing the CCD and making previously stable zones more susceptible to $CaCO_3$ dissolution (Sulpis et al., 2018). In turn, the dissolution of seafloor $CaCO_3$ dissolution leads to an increase in DIC and alkalinity (one unit of DIC per two units of TA, Eqn. 1), causing an increase in pH and a decrease in pCO_2 (Figure 2a and b, Deffeyes diagrams - TA vs DIC plots for pCO_2 and pH respectively; Middleburg et al., 2020). Thus, calcium carbonate mineral dissolution acts as a rapid feedback to transfer carbon from the atmosphere to the oceans, one of Earth's biggest surface carbon reservoirs (Ridgwell, 2007; Colbourn et al., 2015; Renforth and Gideon, 2017; Bogumil et al., 2024).

On longer timescales, CO_2-driven warming also affects other environmental processes such as the hydrological cycle, as increased warming is thought to result in increased precipitation, and the favorability of weathering reactions. These changes lead to increased carbonate and silicate weathering on land, causing increases in river alkalinity fluxes into the ocean. The increase in alkalinity then causes permanent CO_2 drawdown (via carbonate mineral precipitation of the dissolved ocean carbon) and hence stabilizing the system back to its original steady state (Berner and Caldeira, 1997; Kump et al., 2000; Penman et al., 2016; Penman et al., 2020). We note that this perspective is a simplified marine carbonate-centric perspective - there is also a critical role of the terrestrial and marine organic carbon cycle in the Earth system feedback to volcanic forcings since marine productivity is dependent on both the terrestrial riverine fluxes and atmospheric pCO_2 while the reduced ocean oxygenation in warmer oceans affects organic carbon preservation (Hilton and West, 2020; Gernon et al., 2024; Rogger et al., 2024). However, to isolate processes, we will not be focusing on these feedbacks in this study.

Considering the volcanic sulfur pathways, we expect to have both aerosol-driven cooling and a direct effect on ocean pH and alkalinity because sulfate (SO_4^{2-}, sourced from volcanic aerosol and subsequent sulfuric acid rain) is one component of alkalinity (Eqn. 2). The decrease in temperature also affects the ocean temperatures, influencing ocean pH and alkalinity through feedbacks described above (See Figure 2). The temperature change associated with sulfate aerosols is also much more rapid and brief than the greenhouse warming associated with CO_2. This is because the lifetime of sulfate in the stratosphere is short; hence, the atmospheric cooling is expected to persist only slightly longer than the duration of each eruption (Schmidt et al., 2016). However, since the deep ocean mixing timescales can be 1000s of years, there can be a

lag between the surface cooling/warming and the deep ocean response and reduction in the cooling/amplitude (Cessi, 2019; Johnson and Lyman, 2020). Since volcanic aerosol-derived SO_4^{2-} would decrease TA and sulfate has a long residence time in seawater (Halevy et al., 2012; Present et al., 2020), the decrease in TA would lead to a long-term increase in atmospheric pCO_2 (Figure 2c). This is the main sulfur feedback that was included in previous geochemical studies with LOSCAR (Hull et al., 2020).

Although we have a first-order conceptual understanding of how volcanic carbon and sulfur likely affect the environment, the complex causal pathways (see Figure 3 with multiple sequential pathways) mean that the effects of a combination of carbon and sulfur emissions are difficult to predict with pyCO2SYS calculations alone - some changes may be opposite and hence decrease overall change (e.g., cooling vs warming) while others may be additive (e.g., sulfate addition to oceans and pCO_2 increase both decrease TA). Because of the wide range of timescales (up to hundreds of years for sulfate cooling vs hundreds of kiloyears for CO_2 greenhouse warming, Figure 1b), assessing the net timescale of feedbacks without Earth system models is challenging. However, understanding the timescales and response amplitudes is necessary to assess how the eruptions with different durations and gas emission rates affect the environment.

3. Methods

3.1. Geochemical Box Model Setup

For this study, we utilized a geochemical intermediate complexity Earth System model, LOSCAR (Long-term Ocean-atmosphere-Sediment CArbon cycle Reservoir), which models carbon cycle perturbations in the oceans, atmosphere, and ocean sediments (Zeebe, 2012) with a multi-box setup (3 boxes each for each ocean basin along with high latitude and atmospheric boxes). LOSCAR is composed of three main components: the ocean, atmosphere, and marine sediments (Supplementary Figure S1 and Text S1). These boxes are coupled together and interact with each other, connected via the global carbon cycle. The global ocean geometry in the LOSCAR is largely divided into the Pacific (P), Atlantic (A), and Indian (I) ocean basins, with the addition of the Tethys (T) ocean for the Paleogene Period setup (Zeebe, 2012). Each ocean box is subdivided into Low-latitude surface (L), intermediate (M), and Deep boxes (D) based on depth, with circulation occurring within the ocean box. The High-latitude box (H) represents cold surface waters.

In the ocean boxes, ocean circulation and mixing take place based on conveyor circulation and bidirectional mixing among the subdivided boxes. Dissolving or adding $CaCO_3$ into the ocean boxes will result in accumulation or chemical erosion in the sediment boxes. Material exchange with the atmosphere box is also modeled with weathering flux and gas exchange. Weathering processes (e.g., carbonate, silicate weathering) transport CO_2 from the atmosphere to the sediment boxes. In this reaction, atmospheric pCO_2 is consumed, and calcium and bicarbonate ions are provided to the ocean. Precipitation of $CaCO_3$ transports carbon from the ocean to the sediment box. Erosion and accumulation are the main processes within the sediment boxes. LOSCAR calculates the following key environmental tracers in each box: temperature, total DIC, alkalinity (TA), phosphate (PO_4), dissolved O_2, δ13C (although we do not discuss isotopic shifts here), pH, pCO_2, and CCD. Motivated by the interest in LIPs such as the Deccan Traps (Cretaceous-Paleogene boundary) and the North Atlantic Magmatic Province (Paleogene), we used the Paleogene configuration of LOSCAR.

To evaluate the effects of volcanic sulfur emissions on the ocean carbonate system, we modified the original LOSCAR model to include (a) atmospheric effects: sulfate aerosol-driven cooling based on radiative forcing, converted from SO_2 emission flux, and (b) ocean chemistry effects: the effect of sulfur (SO_4^{2-}) on ocean alkalinity (following Hull et al., 2020). In our simulations, we converted volcanic SO_2 emissions (Tg/yr) into a global radiative forcing (W/m^2) by parameterizing the global climate model results (with aerosol growth) from Schmidt et al. (2015). The volcanic sulfur emissions also result in a net decrease in TA (Eqn. 3) through the addition of sulfate ions to the surface ocean boxes (see Supplementary Text S1).

By adopting a lower complexity box model, it is possible to perform long-term modeling (> 1 million years) compared to previous research (e.g., < 20,000 years CESM1 from Black et al., 2018 or < 50,000 years from Landwehrs et al., 2020). With both carbon and sulfur emissions together, we need a model time step of ~0.1 year to properly resolve sulfur-associated effects, because aerosol-driven cooling is rapid and short-lived.

3.2. Model forcings

In order to investigate changes in ocean environmental tracers (pH, ocean temperature, carbonate compensation depth, and alkalinity) due to the eruption of volcanic volatiles, we used various eruption scenarios of an individual LIP eruption (i.e., input forcings). In an eruption scenario, each eruption releases CO_2 and SO_2 into the atmosphere box. We created a range of

eruption scenarios by controlling eruption parameters - (A) mass eruption rate (km^3/yr), aka the volume of lava erupted per year, and (B) duration of eruption (yr). For the mass eruption rate, we span a large physically plausible range, using 5, 10, 20, 30, 50, 75, and 100 km^3/yr (Self et al., 2014; Fendley et al., 2019; Self et al., 2021). To convert these eruption rates into the amount of gas released into the atmospheric box, we use estimates of magmatic carbon and sulfur concentrations from LIP melt inclusions: 14 Tg/km^3 of CO_2 and 6 Tg/km^3 of SO_2 (e.g., Self et al., 2014; Hernandez Nave et al., 2021). For the duration of an eruption, we used the following scenarios: 10, 50, 100, 200, 400, 800, 1600, and 1800 years. Typically, individual continental flood basalt eruptions (i.e., a pulse) are thought to last tens to hundreds of years (Fendley et al., 2019; Mather and Schmidt, 2021; Self et al., 2022). Here, we selected a larger range of values to assess the potential effects from a broad range of volcanic scenarios. For simplicity, we assume that the LIP volcanic gas emissions, especially sulfur, can reach the stratosphere efficiently and thus can cause global-scale effects (Self and Mather, 2014; Glaze et al., 2017). We note that the volcanic plume dynamics of LIP eruptions remain an area of active research and hence, the stratospheric transport efficiency of sulfur may be less than unity - changes in this parameter would at best, rescale all our results, but not change our primary conclusions (Mather and Schmidt, 2021).

By comparing the model results between setups running combined carbon and sulfur emissions (i.e., eruption scenarios including sulfur emission) to results from carbon-only setups (i.e., eruption scenarios without sulfur emission), we are able to assess the effects of sulfur as well as carbon on the marine carbon cycle, especially, highlighting changes in temperature, pH, TA, and the CCD.

4. Results

To highlight the dominant responses and processes, here, we first present results from a single emissions scenario (eruption rate of 50 km^3/yr with an eruption duration of 400 yr), which has a pattern of carbon cycle response that is similar across a wide range of eruption rates and duration. This is followed by a summary of the behavior across the whole parameter space of eruption rates and durations.

4.1. LOSCAR model results from single eruption scenarios

In Figure 4, we show the results of the ocean environmental tracers (e.g., temperature, pH, CCD, and TA) against the elapsed time since the eruption for both carbon-only (C-O) and

carbon plus sulfur (C+S) models. The different ocean basins (Atlantic, Pacific, Indian, and Tethys) and their corresponding depths (i.e., shallow, intermediate, deep) are indicated by different colors and line styles. In the LOSCAR model, all the major ocean basins have the same temperature response, differing only by depth (shallow, intermediate, deep). To further highlight the differences in the results between our two model setups, we subtract the results from the C+S model from the C-O model for each eruption scenario. Below we highlight the observed changes for each environmental tracer of interest.

4.1.1. Oceanic Temperature (°C)

In the C-O model, the ocean temperature rises due to carbon dioxide degassing from volcanic eruptions and consequent increase in atmospheric pCO_2. In our exemplar eruption scenario, we calculate a maximum ocean temperature increase of ~ 0.25°C for the surface and intermediate ocean boxes and ~ 0.2°C for the deep box (Figure 4a). The surface and intermediate ocean boxes warm rapidly following the eruption (years to 10s of years), while the deep ocean takes a few 1000 yr to experience the peak warming. On longer timescales (>10,000 years), the ocean temperatures return to pre-eruption values. This occurs because CO_2 is removed from the atmosphere first by ocean acidification-calcium carbonate dissolution feedback (~ 10,000 years, See Section 2.2) and eventually by terrestrial and marine silicate weathering and calcium carbonate precipitation (~300,000 years).

In the C+S model, released volcanic sulfur has a dominant short-term effect on temperature, and it results in significant ocean cooling (Figure 4b). We note that this case still has the same amount of carbon dioxide emissions as the C-O case. Our exemplar eruption scenario shows a peak decrease of ~5.7 °C in the surface, ~ 4.1°C in the intermediate, and ~2.3°C in the deep box during the eruption. In the deep ocean boxes, we observe that the response time is slower (a few thousand years; Figures 4b and 5a). Correspondingly, the deep ocean also takes longer to return to pre-eruption values than intermediate and shallow boxes. Given the LOSCAR model parameterization, there are no significant differences in temperature responses across the surface boxes (and the same for intermediate and deep boxes). This is clearly illustrated by the overlapping plots in Figure S3a for each ocean depth box for C+S – C-O model differences.

However, in the longer term (10 – 100s of kiloyears), the C+S model results also show warming, driven by the CO_2 release as well as the reduction in TA from the addition of sulfate to seawater. However, the peak amplitude of the warming is less than that of the C-O model

scenario (Figures 4a, b and 5a). This is clearly illustrated by the fact that the peak atmospheric pCO_2 perturbation in the C+S model is about half of that in the C-O model (Figures 4f and 5d). Eventually, silicate weathering helps return the system to the pre-eruption equilibrium state.

The primary temperature behavior we see in the models is determined by the temperature relaxation timescales for each ocean box depth in LOSCAR - 20, 200, and 1,000 years for surface, intermediate, and deep ocean boxes (see supplementary text S1 for details). These ocean mixing and temperature diffusion timescales are consistent with detailed ocean dynamics models and global climate models demonstrating different response timescales for shallow ocean (years to decades) and deep ocean (hundreds to thousands of years) (Gupta and Marshall, 2018).

4.1.2. pH

In our C-O model (Figures 4c, d), pH decreases are observed after the eruption in all ocean boxes (~0.02 pH units in the surface ocean and smaller in the deeper ocean), as expected due to the dissolution of volcanic CO_2 in seawater. Like temperature, the deep ocean box sees a smaller and time-delayed pH response than the volcanic input, likely due to lags introduced by ocean circulation.

In contrast, the C+S model results show a more complex pH response, including both pH increases and decreases over time (Figures 4c, d and 5b). In the shallow ocean boxes, we observe an initial increase in pH followed by a recovery to lower values in ~ 10,000 years. On the other hand, in the intermediate and deep boxes, we see a pH drop immediately after the eruption, followed by a pH increase similar to the surface ocean box (but with a smaller amplitude), and finally relaxation close to a steady state in ~10,000–15,000 years. Thus, when comparing the difference in pH perturbations between the C+S and C-O model, we see that the surface ocean boxes always see a pH increase compared to the C-O model. In contrast, the intermediate and deep ocean boxes (Atlantic, Indian, Tethys - Figure 5b) see both a stronger pH decrease and a subsequent pH increase in the C+S models. We also find that the response in the Pacific Ocean box is slightly different compared to the other ocean boxes - the deep Pacific does not have a pronounced initial drop in pH compared to other deep ocean boxes. These differences are likely because of different initial TA, alkalinity, and ocean temperatures and the prescribed spatial pattern of ocean circulation in LOSCAR. Overall pH changes in the C+S model are more temporally complex and variable compared to the C-O model.

4.1.3. Carbonate Compensation Depth and Total Alkalinity

Figure 4e shows the CCD changes in the four ocean basins (i.e., Atlantic, Pacific, Indian, and Tethys) following the volcanic carbon and carbon and sulfur emissions, respectively. In the model results, the overall CCD in both the model scenarios initially becomes shallower, although the amplitude of CCD change is different across ocean basins. This is expected since ocean acidification leads to calcium carbonate dissolution and a corresponding increase in TA (Figure 2). This process represents the fast ocean chemical buffering response to atmospheric pCO_2 increases and occurs over timescales of 5,000–20,000 years (Section 2.2). On longer timescales, the CCD in the C-O model becomes deeper than the pre-eruption state - this allows the removal of carbon from the ocean-atmosphere system by seafloor sedimentary carbon burial and silicate weathering (Bogumil et al., 2024).

Although we see similar overall CCD behavior in the C+S model, the CCD changes are much faster/abrupt (~5,000-10,000-year timescale) and also have a larger magnitude. These are coincident with the strong decreases in pH in the deep ocean boxes. Correspondingly, TA shows a much larger and faster increase in the C+S models in the deep ocean (Supplemetary Figure S2). In contrast, the shallow and intermediate ocean boxes in the C+S model show an initial TA decrease after the eruption partially due to sulfate addition in the surface ocean. This is followed by an increase in TA over a few 1000 yr timescale before relaxation to an equilibrium state.

In both C+S and C-O models, we see that the CCD shallowing of the Atlantic and Indian oceans is more pronounced than that of the Pacific and Tethys ocean boxes. This is likely related to different initial TA-DIC states of the deep ocean boxes which in turn lead to a deeper initial CCD for the Atlantic ocean. Overall, we find a more dynamic and faster CCD response in the C+S model. This is also reflected by the faster changes in TA and DIC in the C+S models (Supplementary Figures S2 and S3) across the different ocean boxes.

To further illustrate the significantly different ocean marine carbonate chemistry dynamics in the C-O and C+S models, we show the time evolution of the models in the TA-DIC space (Figure 6; Supplementary Data S3). This clearly illustrates that the two models follow distinct trajectories, with the C+S model exhibiting initial sulfate-associated TA change and DIC increase, likely due to colder temperatures. This is followed by the effect of calcium carbonate dissolution, which increases TA and DIC and eventually seafloor carbonate burial to return the system back to equilibrium. We find that the distinction between the C-O and C+S models is

stronger in the shallow ocean box. This is expected given the stronger temperature perturbation in the upper ocean from sulfate-aerosol cooling. The exact trajectories are a consequence of the coupled ocean carbon cycle in LOSCAR and are thus complex. However, the results clearly illustrate visually the significant differences between the C-O and the C+S models in the context of primary marine carbon cycle parameters.

4.1.4 Atmospheric pCO_2

In the C-O model, the carbon dioxide degassing from volcanic eruptions leads to an increase in in atmospheric pCO_2 (Figure 4f – solid line). Subsequently, the atmospheric pCO_2 returns back to pre-eruption state over 10s-100s of kyr due to the combined effect of carbonate and silicate weathering cycles. In the C-S case, we see an initial rapid decrease in atmospheric carbon dioxide in C+S model (Figure 4f – dashed line) despite volcanic carbon emissions. This is likely due to enhanced dissolution of CO_2 in colder surface ocean waters (Figure 4a – dashed line). When the surface ocean temperatures relax back to pre-eruption state, the atmospheric increases (even though the eruption has stopped much earlier) due to atmosphere-ocean exchange. However, the peak atmospheric in the C+S model is lower than the C-O model, even though they have the same overall volcanic carbon dioxide emissions. These results highlight the significant indirect impact of volcanic S emissions on the climate by coupling through the inorganic marine carbon cycle. We also find a similar type of behavior for the dissolved ocean oxygen content, but inverted in sign. The dissolved oxygen decreases in the C-O model due to an increase in ocean temperatures. In contrast, it initially increases in the C+S model due to reduced temperatures and increased seawater dissolution, followed by a return to a similar response as the C-O model over long timescales (See Supplementary Data S2; Figure 3).

4.2. Environmental tracers vs total eruption volume

Next, we analyze the overall trends in changes in temperature, pH, and CCD as a function of eruption duration, eruption rate, and total eruption volume (Figures 7 and 8, Supplementary Figures S4-15; Supplementary Data S4). Here, we show results for the Pacific and the Atlantic Ocean basins since they are the largest ocean basins, and the changes are representative of global averaged behavior.

Overall, we see that the changes in environmental tracers are strongly dependent on the total eruption volume, and the shallower the ocean depth, the greater the perturbation. For

instance, the shallow ocean boxes experience stronger maximum cooling for larger eruption volumes in contrast to intermediate and deep ocean boxes (Figure 7). Additionally, the C-O model's maximum warming is larger than the C+S models across the parameter space. This result suggests that volcanic sulfur indirectly affects ocean warming long after the direct effect of cooling has dissipated.

Considering the ocean pH, the eruption volume similarly primarily controls the behavior (Figure 8), though there is a fair bit of scatter at high erupted volumes. The pH reduction in the C+S models is typically smaller than the C-O model for the Pacific Ocean boxes but it is larger in the Atlantic Ocean box (similar to the results discussed earlier). Furthermore, we uniquely see a large increase in pH compared to the initial state in the C+S model, likely due to the temperature dependence of marine carbonate equilibrium coefficients (Figure 2). Finally, CCD changes in the Pacific and Atlantic both depend on erupted volume, but with different relationships (Supplementary Figure S4). The CCD shoaling is much stronger in the C+S models with the Atlantic Ocean (deepest CCD) experiencing the first changes followed by the Pacific with increasing eruption volumes. This is potentially related to the different structures of ocean circulation in these ocean basins - the Atlantic has a faster overturning circulation that also leads to a stronger pH perturbation in the deep ocean.

When we compare eruption scenarios that have the same total eruptive volume but differing eruption duration, we see that a short-duration, high-mass eruption rate (large amount of gas emissions per year) results in larger magnitude temperature changes in shallow ocean model responses compared to a long-duration eruption with a smaller mass eruption rate (Supplementary Figure S5). However, this is not the case for deep ocean boxes wherein a long-lived eruption (comparable to timescales of ocean overturning circulation, ~ few 1000 years) can cool the deep ocean more than a large but short-lived eruption, thus affecting ocean CCD and pH of deep ocean box in a complex manner (Supplementary Figures S6-S9).

Thus, overall we find that both the eruption rate and duration are important, depending on the environmental tracer of interest, and eruption volume alone does not capture the full carbon cycle response (Supplementary Figures S10-S15). Analyzing the exact reasons for the differences between different scenarios, especially the structure of the CCD responses across different ocean basins, is beyond the scope of the current paper since it depends on the nature of

ocean mixing and initial bathymetric distribution of the basins (Bogumil et al., 2024). Our results across the parameter space show the diversity of responses in the environmental tracers for different eruption parameters with significant differences between the C+S and C-O models.

5. Discussion

5.1. Counterintuitive effects of temperature-dependent equilibrium coefficient on pH:

Looking at the C+S model pH results (Figure 4c and 4d; Figure 5b), pH responses vary with the ocean depths and over time. Intuitively, following a volcanic eruption, pH in the surface ocean should decrease due to ocean acidification from the addition of CO_2 and sulfuric acid. However, the results show that pH actually increases in the shallow ocean boxes. This is most likely because the equilibrium coefficients of the various DIC species are temperature-dependent variables, and a decrease in temperature (for a constant TA and DIC) results in an increase in pH (Figure 2). Although the input of acids (sulfate, dissolved CO_2) into the surface water likely has an effect, the temperature effect is larger, and hence, there is a net increase in pH.

Since diffusion in the environmental tracers (DIC, TA) in seawater is much smaller than temperature, thermohaline circulation (i.e., physical transport of water mass) can transport carbonate ionic species between ocean boxes more efficiently than temperature changes (Sharqawy et al., 2010; Zeebe, 2011; Supplementary Text S1). Thus, the intermediate and deep ocean boxes see the changes due to acidification (CO_2 and SO_4^{2-} input) more quickly than the temperature changes, resulting in an initial decrease in pH. This is further enhanced by increased solubility of CO_2 in seawater at lower temperatures at the surface, which results in an increase in DIC which is then transported to the deeper ocean. Then, an increase in pH follows after a few hundred years, due to the combined effects of a) rapid carbonate mineral dissolution at the seafloor, increasing TA and shallowing the CCD, and b) the temperature decrease finally reaching the deeper ocean from the surface. Figure 3 shows a schematic description of this feedback loop while Figure 6 shows the time-trajectory of the C-O and C+S model for two representative ocean boxes.

In summary, in the C+S model, the effects of cooling on temperature-dependent DIC-species equilibrium coefficients lead to faster transport of atmospheric carbon into the ocean than in the C-O model. Furthermore, the feedback described above leads to a rapid shoaling of the CCD and then a subsequent rebound in pH within a few hundred to a thousand years. Overall,

623 the calcium carbonate dissolution feedback process, which occurs in the C-O model over 5,000–
624 20,000 years, occurs much more rapidly in the C+S model.

625 Furthermore, because carbon is sequestered into the ocean faster in the C+S model, the
626 overall long-term warming is less, even long after the sulfate aerosol-driven cooling is over. This
627 is because the peak atmospheric carbon dioxide is lower in the C+S model due to the rapid
628 sequestration of some volcanic C in the ocean compared to the C-O model (Figure 4f). Thus,
629 even with the same total volcanic carbon emissions, the climate response of the C+S model is
630 strikingly different. This result contrasts with previous studies, (e.g., Hull et al., 2020), that only
631 considered the effects of sulfur on ocean alkalinity and hence found that volcanic sulfur caused
632 enhanced warming over long timescales. *Overall, our results illustrate that the timescale*
633 *separation assumption for volcanic carbon and sulfur impacts, inherent in a number of previous*
634 *studies, does not always apply.* These results have important implications in terms of interpreting
635 paleoclimate proxies, especially high-resolution records of potential LIP associated cooling and
636 warming (e.g., O'Connor et al., 2024).

637 5.2. Identifying dominant effects within the causal diagram:

638 Using our model results, we were able to identify the dominant effects associated with
639 volcanic carbon and sulfur emissions in the context of marine carbonate chemistry as well as the
640 associated timescales. By comparing the results from the C-O vs. the C+S models, we can isolate
641 the impacts of volcanic sulfur emissions on the ocean-atmosphere system. We used these model
642 results to update the causal diagram shown in Figure 3, focusing on the dominant feedback
643 loops.

644 The causal diagram uses distinct colors to indicate different timescales for various
645 processes. Relatively rapid events (year to decade scale), such as acid rain or sulfate aerosol
646 cooling, are displayed using red arrows. Century-scale intermediate processes include
647 temperature, pH, TA drops, and rapid shoaling of the CCD after the eruptions (green arrows).
648 Relatively long-term reactions (i.e., more than 1000 yrs) are indicated by navy blue arrows. The
649 causal diagram provides a visual summary of the processes described in the previous sections
650 and thus can act as a mechanistic framework to assess how large eruptions affect the
651 environment.

A key conclusion from our results and the causal diagram is the importance of appropriate time resolution in the carbon cycle models (Figure 3). For instance, the dominant processes in the C+S model include ocean temperature change and CCD shoaling, both of which occur at intermediate (~century) timescales. Consequently, the temporal resolution of the model is very important. Models with a few 1000-year time steps (e.g., Cox and Keller, 2023) will not resolve these processes, and this may strongly affect the long-term behavior. In our models, we use a time step of a fraction of a year to fully resolve the short-term cooling effects from sulfate aerosol and its effects on marine carbonate chemistry due to temperature-dependent equilibrium constants. Although more computationally expensive than a longer time step, especially when models need to run for hundreds of kiloyears to millions of years, our results suggest that high temporal resolution is necessary to capture the dynamics resulting from very rapid processes, which (as discussed in the previous section) do impact the much longer-term carbon cycle.

5.3. Importance of multiple eruptions:

In this study, we have focused on the effects of a single large eruption on the marine carbon cycle. In reality, LIPs are characterized by multiple individual eruptions over a million-year timescale (Sprain et al., 2019; Black et al., 2021; Mittal et al., 2021; Self et al., 2021). Thus, to compare our model results with paleo-environmental datasets, we need to consider scenarios with multiple eruptions and evaluate the importance of other eruption parameters such as the typical time between eruptions and the total number of eruptions. Although we do not model this explicitly, our results do provide some perspective on what we might expect for multi-eruption scenarios, since we have determined the key response timescales. When the time between eruptions is shorter than the timescale over which the large responses persist, e.g., effects on CCD, pH, and temperature, the effect of multiple eruptions will be additive and complementary (e.g., see Figure 4 and Supplementary Dataset S2 for response timescales). In contrast, if the eruption frequency is much lower, each of the multiple eruptions will be effectively independent. Since the deep ocean responses are typically longer duration (due to ocean mixing; Figure 4b), there is a higher likelihood of additive responses in the deep ocean from multiple eruptions (Gupta and Marshal, 2018).

Additionally, our results for marine CCD and pH show a series of complex changes within the first few thousand years after an eruption (Figure 5b,c). Geochemical and volcanological estimates of LIP eruption recurrence intervals suggest that subsequent eruptions

likely occurred within that time interval (e.g., Mittal et al., 2022; Fendley et al., 2019). In that case, the marine carbon cycle would experience large, rapid, and repeated perturbations, with significant implications for the ecosystem impact of the eruptions and their potential to trigger a mass extinction (e.g., Close et al., 2020; Foster et al., 2023; Monarrez et al., 2023; Payne et al., 2023). Analyzing the response and feedbacks for multiple closely-spaced eruptions (within a few thousand years) is beyond the scope of the present study, but would be a fruitful avenue for future work.

5.4. Role of ocean dynamics and biological feedbacks:

Our study has focused on understanding how these LIP volatiles impact climate change by examining individual environmental tracers and their relationships specifically in the context of ocean geochemistry. To simplify our models and gain mechanistic insights, we excluded certain factors such as physical ocean/atmosphere dynamics and biological processes. However, as a next step, coupling the chemical, physical, and biological processes is needed to understand the net effect of large volcanic eruptions with carbon and sulfur emissions. In particular, the strong surface temperature changes in our results would affect the ocean-atmosphere dynamics. For example, previous work by Black et al., (2018) shows that volcanic cooling enhances the rate of the global ocean overturning circulation. However, their work did not examine the consequent effects on marine carbonate chemistry (e.g., TA, DIC) and biological productivity. Since the ocean pH and CCD responses are dependent on temperature and ocean circulation in our model (See Section 5.1, Figure 2), understanding the coupled feedbacks using a physical-chemical model is a key direction for future work.

Additionally, future studies should consider the coupling between sulfate aerosols and stratospheric water vapor and its effect on surface cooling and warming. Guzewich et al. (2022 and 2024) found that sulfate aerosols can locally heat up the stratosphere and thus increase the water vapor content in the lower stratosphere. Since water vapor is a greenhouse gas (Maycock et al., 2021), it can cause global warming following the stratospheric cooling from the eruptions given the longer stratospheric residence time of water vapor compared to aerosols. Stratospheric water vapor can in turn affect stratospheric ozone and atmospheric dynamics, leading to various feedbacks (which can lead to warming or cooling) that need to be carefully analyzed and then parameterized in long-term carbon cycle models (Wang et al., 2023; Fleming et al., 2024). Finally, changes in ocean temperature and chemistry would significantly affect marine

ecosystems and productivity as biological pump efficiency (rates of carbonate and organic carbon remineralization in the water column). These and other important dynamical feedbacks would need to be coupled to the work we have done in this study to develop a full mechanistic casual diagram framework and interpret paleoclimate records; our work provides a baseline for the chemistry of the carbon cycle feedbacks.

6. Conclusions

In this paper, we conducted model experiments to evaluate whether sulfate aerosol-driven cooling during continental flood basalt eruptions has long-term effects on the marine carbon cycle. We used the LOSCAR intermediate complexity carbon cycle model and compared the model results for running a scenario with only CO_2 emissions with those using a scenario involving both CO_2 and SO_4^{2-} emissions (which we assume reach the stratosphere). We found that volcanic sulfur has a significant impact on all the environmental tracers in the model - temperature, pH, TA, DIC, and CCD.

In our carbon and sulfur model results, we find some counterintuitive behavior, such as the increase in pH in the surface ocean immediately following an eruption. However, the reason for this change became clear when considering the impact of temperature decrease on DIC species equilibria. Although this sulfate aerosol-driven cooling is brief (<~500 years), its effects on marine carbonate chemistry persist for much longer, for example, the peak amount of warming is lower in the carbon and sulfur model scenario relative to that with carbon emissions alone.

In conclusion, our results validate our hypothesis that volcanic sulfur emissions can have a significant long-term effect on the marine carbon cycle (pH, alkalinity, and carbonate compensation depth) and not just on short (tens to hundreds of years) timescales. The effects of volcanic sulfur are not simply additive to the impact of volcanic carbon alone, highlighting the importance of analyzing them both jointly, rather than individually for large eruptions, particularly flood basalt eruptions. Furthermore, high temporal resolution (~0.1 yr) is needed to properly represent the volcanic effects on the marine carbon cycle. We also develop a causal, mechanistic framework to understand the effects of combined carbon and sulfur emissions. This framework can be extended to include physical (atmospheric, ocean dynamics) and biological

743 processes in the future to help develop a comprehensive understanding of how large volcanic
744 eruptions affect the environment.

745 **Figure Captions**
746
747 **Figure 1**. (a) A schematic illustration showing the direct and indirect environmental
748 effects of volcanic carbon and sulfur emissions from Large Igneous Province (LIP) volcanism,
749 modified after Clapham and Renne (2019). (b) Timescale of earth system processes and
750 geological events affecting the surface environmental change. We note the potential timescales
751 for forcings from individual eruptions and large igneous province emplacement at the bottom.
752 Modified after Rohling et al. (2018).

753 **Figure 2.** Alkalinity (TA) versus dissolved inorganic carbon (DIC) plots, calculated
754 using CO2SYS, for the very shallow ocean (~100 m) and 10°C with corresponding equilibrium
755 values shown as colors for atmospheric pCO_2 (a) and pH (b). Effects of seawater temperature on
756 the equilibrium pCO_2 (c) and pH (d) as a function of TA for a fixed DIC value (2 mmol/kg) and
757 shallow ocean depths (~ 100 m).

758 **Figure 3.** Causal diagram showing the dominant effects and relative reaction rate from
759 LOSCAR model results. The red arrows indicate short-term processes (~tens of years), the green
760 arrows intermediate (~hundreds of years), and the dark blue arrows indicate long-term processes
761 (~thousands of years). Blue stars highlight the dominant effects in the model results.
762 Temperature decrease, pH increase, and TA increase are the dominant environmental effects of
763 the combined sulfur and carbon model. The yellow highlighted box shows the dominant reaction
764 flow in the model results.

765 **Figure 4.** Plots of several environmental tracers responding to gas equivalents of an
766 eruption of 50 km^3/yr of basalt (with assumed gas content of 14 Tg/km^3 of CO_2 and 6 Tg/km^3 of
767 SO_2), emitted over 400 years, for carbon-only (C-only, solid lines) and carbon and sulfur (C+S,
768 dashed lines) model results. Each plot spans 5000 years before the eruption to 30,000 years since
769 eruption initiation to highlight initial changes (c.f. the total model duration is 2,000,000 years).
770 (a) and (b) show the temperature in the shallow and deep ocean, respectively (note these
771 temperatures are the same for the major ocean basins and only vary as a function of ocean
772 depth). (c) and (d) show pH for the Pacific and Atlantic oceans as representative examples. (e)

773 shows the CCD response for each major ocean basin. (f) shows atmospheric pCO_2 for the C-only
774 and C+S models.

775 **Figure 5**. Differences in temperature (a), pH (b), CCD (c), and atmospheric pCO_2 (d)
776 between the combined carbon and sulfur (C+S) model and the carbon-only (C-only) model for an
777 eruption of 50 km^3/yr and duration of 400 years. The plots are illustrated by subtracting the value
778 for the relevant parameter in the C-only model results from the C+S model results. Hence,
779 negative (positive) values indicate lower (higher) environmental tracer values in the combined
780 model than in the carbon-only model.
781
782 **Figure 6.** Pathway plots for alkalinity (TA) against dissolved inorganic carbon (DIC)
783 plots with temperature (color) in the Pacific surface (a) and deep (b) ocean boxes spanning the
784 model results for an eruption of 50 km^3/year and duration of 400 years. The path represents the
785 total ~100,000-year duration of the model run after eruption initiation. Both C-only and C+S
786 models have the same starting TA, DIC, and temperature values. Note that (a) and (b) have
787 different temperature scales. The passage of time for the carbon-only (C-only; pink arrows) and
788 the combined carbon and sulfur (C+S; green arrows) models are shown as arrows. Important
789 time points are indicated, including maximum and minimum temperature, eruption start and end,
790 and model end.
791
792 **Figure 7.** Plots of maximum warming and maximum cooling in relation to the total
793 volume of the eruption (km^3). Note the difference in the y-axis scale for (a) and (b) and that the
794 temperatures are the same for the major ocean basins and only vary as a function of ocean depth.
795 Maximum warming (cooling) is the maximum difference between the initial and highest (lowest)
796 temperature values for a particular model result (C-only: red circles; C+S: blue circles and
797 squares). Maximum cooling is not plotted for the C-only model because cooling effects are
798 insignificant.

799 **Figure 8.** Plots of maximum pH increase and decrease in relation to the total volume of
800 the eruption (km^3), for the Pacific and Atlantic ocean basins, including the shallow, intermediate,
801 and deep ocean boxes. The maximum pH increase (decrease) is the difference between the initial
802 and highest (lowest) pH values for a particular model result (C-only: red circles and squares;
803 C+S: blue circles and squares).

Acknowledgments

HJC and CJS acknowledge funding from National Science Foundation (NSF) grant #2321344. CJS additionally acknowledges funding from NSF grants #2237807, #2245629, #2054605, and #2016763. TM acknowledges funding from PSU. We acknowledge computational support from HiPerGator super computing facility at UF. We acknowledge Richard Zeebe for providing a copy of the LOSCAR code for the work in this study. We acknowledge Steve Self, Paul Renne, Mark Richards, and Matthew Bogumil for helpful discussions about this work and LOSCAR modeling.

CRediT Roles:

HJC: Data curation, formal analysis, investigation, visualization, writing-original draft, and software. CJS: Funding acquisition, investigation, project administration, resources, supervision, and writing-review and editing. TM: Conceptualization, formal analysis, investigation, methodology, project administration, software, supervision, validation, visualization, and writing-review and editing. IF: Conceptualization, investigation, methodology, validation, visualization, and writing-review and editing.

Open Research

All data (model output files as well as python scripts) are available at Cheong et al., 2024. The original LOSCAR code was graciously provided to us by Richard Zeebe. Additional figures and model results are also available within the supplemental information.

References

Berner, R. A., & Caldeira, K. (1997). The need for mass balance and feedback in the geochemical carbon cycle. Geology, 25(10), 955-956. https://doi.org/10.1130/0091-7613(1997)025<0955:TNFMBA>2.3.CO;2

Black, B. A., Neely, R. R., Lamarque, J.-F., Elkins-Tanton, L. T., Kiehl, J. T., Shields, C. A., et al. (2018). Systemic swings in end-Permian climate from Siberian Traps carbon and sulfur outgassing. Nature Geoscience, 11(12), 949-954. https://doi.org/10.1038/s41561-018-0261-y

Black, B. A., Karlstrom, L., & Mather, T. A. (2021). The life cycle of large igneous provinces. Nature Reviews Earth & Environment, 2(12), 840-857. https://doi.org/10.1038/s43017-021-00221-4

Black, B. A., Karlstrom, L., Mills, B. J., Mather, T. A., Rudolph, M. L., Longman, J., & Merdith, A. (2024). Cryptic degassing and protracted greenhouse climates after flood basalt events. Nature Geoscience, 1-7.

Bogumil, M., Mittal, T., & Lithgow-Bertelloni, C. (2024). The effects of bathymetry on the long-term carbon cycle and CCD. Proceedings of the National Academy of Sciences, 121(21), e2400232121. https://doi.org/10.1073/pnas.2400232121

Callegaro, S., Baker, D. R., Renne, P. R., Melluso, L., Geraki, K., Whitehouse, M. J., et al. (2023). Recurring volcanic winters during the latest Cretaceous: Sulfur and fluorine budgets of Deccan Traps lavas. Science advances, 9(40), eadg8284. https://doi.org/10.1126/sciadv.adg8284

Cessi, P. (2019). The global overturning circulation. Annual Review of Marine Science, 11(1), 249-270. https://doi.org/10.1146/annurev-marine-010318-095241

Cheong, H. J., Mittal, T., Sprain, C., & Isabel, F. (2024). supplementary material for "Analyzing the joint effect of volcanic carbon and sulfur emissions on the marine carbon cycle", for Geochemistry, Geophysics, Geosystems [Data set]. https://doi.org/10.5281/zenodo.13760340

Clapham, M. E., & Renne, P. R. (2019). Flood basalts and mass extinctions. Annual Review of Earth and Planetary Sciences, 47(1), 275-303. https://doi.org/10.1146/annurev-earth-053018-060136

862 Close, R. A., Benson, R. B., Saupe, E. E., Clapham, M. E., & Butler, R. J. (2020). The spatial
863 structure of Phanerozoic marine animal diversity. *Science*, *368*(6489), 420-424.
864
865 Colbourn, G., Ridgwell, A., & Lenton, T. (2015). The time scale of the silicate weathering
866 negative feedback on atmospheric CO_2. Global Biogeochemical Cycles, 29(5), 583-596.
867 https://doi.org/10.1002/2014GB005054
868
869 Courtillot, V. E., & Renne, P. R. (2003). On the ages of flood basalt events. Comptes Rendus
870 Geoscience, 335(1), 113-140. https://doi.org/10.1016/S1631-0713(03)00006-3
871
872 Courtillot, V. (2002). Evolutionary catastrophes: the science of mass extinction: Cambridge
873 University Press.
874
875 Cox, A. A., & Keller, C. B. (2023). A Bayesian inversion for emissions and export productivity
876 across the end-Cretaceous boundary. Science, 381(6665), 1446-1451.
877 https://doi.org/10.1126/science.adh3875
878
879 Delmelle, P. (2003). Environmental impacts of tropospheric volcanic gas plumes. Geological
880 Society, London, Special Publications, 213(1), 381-399.
881 https://doi.org/10.1144/GSL.SP.2003.213.01.23
882
883 Ernst, R. E. (2014). Large igneous provinces: Cambridge University Press.
884 https://doi.org/10.1017/CBO9781139025300
885
886 Fay, A. R., McKinley, G. A., Lovenduski, N. S., Eddebbar, Y., Levy, M. N., Long, M. C., et al. (2023).
887 Immediate and Long-Lasting Impacts of the Mt. Pinatubo Eruption on Ocean Oxygen and
888 Carbon Inventories. Global Biogeochemical Cycles, 37(2), e2022GB007513.
889 https://doi.org/10.1029/2022GB007513
890

Fendley, I. M., Mittal, T., Sprain, C. J., Marvin-DiPasquale, M., Tobin, T. S., & Renne, P. R. (2019). Constraints on the volume and rate of Deccan Traps flood basalt eruptions using a combination of high-resolution terrestrial mercury records and geochemical box models. Earth and Planetary Science Letters, 524, 115721. https://doi.org/10.1016/j.epsl.2019.115721

Fleming, E. L., Newman, P. A., Liang, Q., & Oman, L. D. (2024). Stratospheric temperature and ozone impacts of the Hunga Tonga-Hunga Ha'apai water vapor injection. Journal of Geophysical Research: Atmospheres, 129(1), e2023JD039298. https://doi.org/10.1029/2023JD039298

Foster, W. J., Allen, B. J., Kitzmann, N. H., Münchmeyer, J., Rettelbach, T., Witts, J. D., ... & Dunhill, A. M. (2023). How predictable are mass extinction events?. *Royal Society open science*, *10*(3), 221507.

Gattuso, J.P., Magnan, A., Billé, R., Cheung, W.W., Howes, E.L., Joos, F., Allemand, D., Bopp, L., Cooley, S.R., Eakin, C.M. and Hoegh-Guldberg, O., 2015. Contrasting futures for ocean and society from different anthropogenic CO_2 emissions scenarios. Science, 349(6243), p.aac4722.

Gernon, T., Mills, B., Hincks, T., Merdith, A., Alcott, L., Rohling, E., & Palmer, M. (2024). Solid Earth forcing of Mesozoic oceanic anoxic events. Nature Geoscience. https://doi.org/10.1038/s41561-024-01496-0

Glaze, L. S., Self, S., Schmidt, A., & Hunter, S. J. (2017). Assessing eruption column height in ancient flood basalt eruptions. Earth and Planetary Science Letters, 457, 263-270. https://doi.org/10.1016/j.epsl.2014.07.043

Gupta, M., & Marshall, J. (2018). The climate response to multiple volcanic eruptions mediated by ocean heat uptake: Damping processes and accumulation potential. Journal of Climate, 31(21), 8669-8687. https://doi.org/10.1175/JCLI-D-17-0703.1

Guzewich, S. D., Oman, L. D., Richardson, J. A., Whelley, P. L., Bastelberger, S. T., Young, K. E., et al. (2022). Volcanic climate warming through radiative and dynamical feedbacks of SO_2 emissions. Geophysical Research Letters, 49(4), e2021GL096612. https://doi.org/10.1029/2021GL096612

Guzewich, S. D., Oman, L. D., Colarco, P. R., Richardson, J. A., Whelley, P. L., Fauchez, T. J., et al. (2024). A potential surface warming regime for volcanic super-eruptions through stratospheric water vapor increases. Journal of Geophysical Research: Atmospheres, 129(13), e2023JD038667. https://doi.org/10.1029/2023JD038667

Halevy, I., Peters, S. E., & Fischer, W. W. (2012). Sulfate burial constraints on the Phanerozoic sulfur cycle. Science, 337(6092), 331-334. https://doi.org/10.1126/science.1220224

Hernandez Nava, A., Black, B. A., Gibson, S. A., Bodnar, R. J., Renne, P. R., & Vanderkluysen, L. (2021). Reconciling early Deccan Traps CO2 outgassing and pre-KPB global climate. Proceedings of the National Academy of Sciences, 118(14), e2007797118. https://doi.org/10.1073/pnas.2007797118

Hilton, R. G., & West, A. J. (2020). Mountains, erosion and the carbon cycle. Nature Reviews Earth & Environment, 1(6), 284-299. https://doi.org/10.1038/s43017-020-0058-6

Hull, P. M., Bornemann, A., Penman, D. E., Henehan, M. J., Norris, R. D., Wilson, P. A., et al. (2020). On impact and volcanism across the Cretaceous-Paleogene boundary. Science, 367(6475), 266-272. https://doi.org/10.1126/science.aay5055

Humphreys, M. P., Lewis, E. R., Sharp, J. D., & Pierrot, D. (2022). pyCO2SYS v1. 8: Marine carbonate system calculations in Python. Geoscientific Model Development, 15(1), 15-43. https://doi.org/10.5194/gmd-15-15-2022

949 Johnson, G. C., & Lyman, J. M. (2020). Warming trends increasingly dominate global ocean.
950 Nature Climate Change, 10(8), 757-761. https://doi.org/10.1038/s41558-020-0822-0
951
952 Kasbohm, J., Schoene, B., & Burgess, S. (2021). Radiometric constraints on the timing, tempo,
953 and effects of large igneous province emplacement. Large igneous provinces: A driver of global
954 environmental and biotic changes, 27-82. https://doi.org/10.1002/9781119507444.ch2
955
956 Kump, L. R., Brantley, S. L., & Arthur, M. A. (2000). Chemical weathering, atmospheric CO_2, and
957 climate. Annual Review of Earth and Planetary Sciences, 28(1), 611-667.
958 https://doi.org/10.1146/annurev.earth.28.1.611
959
960 Landwehrs, J. P., Feulner, G., Hofmann, M., & Petri, S. (2020). Climatic fluctuations modeled for
961 carbon and sulfur emissions from end-Triassic volcanism. Earth and Planetary Science Letters,
962 537, 116174. https://doi.org/10.1016/j.epsl.2020.116174
963
964 Le Hir, G., Fluteau, F., Suchéras-Marx, B., & Goddéris, Y. (2020). Amplifying factors leading to
965 the collapse of primary producers during the Chicxulub impact and Deccan Traps eruptions.
966 Mass Extinctions, Volcanism, and Impacts: New Developments, 544, 223.
967 https://doi.org/10.1130/2020.2544(09)
968
969 Mather, T. A., & Schmidt, A. (2021). Environmental effects of volcanic volatile fluxes from
970 subaerial large igneous provinces. Large igneous provinces: A driver of global environmental
971 and biotic changes, 103-116. https://doi.org/10.1002/9781119507444.ch4
972
973 Maycock, A. C., Smith, C. J., Rap, A., & Rutherford, O. (2021). On the structure of instantaneous
974 radiative forcing kernels for greenhouse gases. Journal of the Atmospheric Sciences, 78(3), 949-
975 965. https://doi.org/10.1175/JAS-D-19-0267.1
976

977 Middelburg, J. J., Soetaert, K., & Hagens, M. (2020). Ocean alkalinity, buffering and
978 biogeochemical processes. Reviews of Geophysics, 58(3), e2019RG000681.
979 https://doi.org/10.1029/2019RG000681
980
981 Mittal, T., Richards, M. A., & Fendley, I. M. (2021). The magmatic architecture of continental
982 flood basalts I: Observations from the Deccan Traps. Journal of Geophysical Research: Solid
983 Earth, 126(12), e2021JB021808. https://doi.org/10.1029/2021JB021808
984
985 Mittal, T., & Richards, M. A (2021). The magmatic architecture of continental flood basalts: 2. A
986 new conceptual model." Journal of Geophysical Research: Solid Earth 126, no. 12 (2021):
987 e2021JB021807.
988
989 Monarrez, P. M., Heim, N. A., & Payne, J. L. (2023). Reduced strength and increased variability
990 of extinction selectivity during mass extinctions. *Royal Society Open Science*, *10*(9), 230795.
991
992 O'Connor, Lauren K., Rhodri M. Jerrett, Gregory D. Price, Tyler R. Lyson, Sabine K. Lengger,
993 Francien Peterse, and Bart E. van Dongen. "Terrestrial evidence forvolcanogenic sulfate-driven
994 cooling event~ 30 kyr before the Cretaceous–Paleogene mass extinction." *Science advances* 10,
995 no. 51 (2024): eado5478.
996 Payne, J. L., Al Aswad, J. A., Deutsch, C., Monarrez, P. M., Penn, J. L., & Singh, P. (2023).
997 Selectivity of mass extinctions: patterns, processes, and future directions. *Cambridge Prisms:*
998 *Extinction*, *1*, e12.
999
1000 Penman, D. E., Turner, S. K., Sexton, P. F., Norris, R. D., Dickson, A. J., Boulila, S., et al. (2016). An
1001 abyssal carbonate compensation depth overshoot in the aftermath of the Palaeocene-Eocene
1002 Thermal Maximum. Nature Geoscience, 9(8), 575-580. https://doi.org/10.1038/ngeo2757
1003

Penman, D. E., Rugenstein, J. K. C., Ibarra, D. E., & Winnick, M. J. (2020). Silicate weathering as a feedback and forcing in Earth's climate and carbon cycle. Earth-Science Reviews, 209, 103298. https://doi.org/10.1016/j.earscirev.2020.103298

Present, T. M., Adkins, J. F., & Fischer, W. W. (2020). Variability in sulfur isotope records of Phanerozoic seawater sulfate. Geophysical Research Letters, 47(18), e2020GL088766. https://doi.org/10.1029/2020GL088766

Rader, E., Peters, S., Vanderkluysen, L., Clarke, A. B., & Sheth, H. (2024). Morphological transitions between lobate resurfacing and distal breakout lava flows in flood basalts: insights from analog experiments. Bulletin of Volcanology, 86(1), 1-12. https://doi.org/10.1007/s00445-023-01693-6

Renforth, P., & Henderson, G. (2017). Assessing ocean alkalinity for carbon sequestration. Reviews of Geophysics, 55(3), 636-674. https://doi.org/10.1002/2016RG000533

Ridgwell, A. (2007). Interpreting transient carbonate compensation depth changes by marine sediment core modeling. Paleoceanography, 22(4). https://doi.org/10.1029/2006PA001372

Robock, A. (2000). Volcanic eruptions and climate. Reviews of Geophysics, 38(2), 191-219. https://doi.org/10.1029/1998RG000054

Rogger, J., Judd, E. J., Mills, B. J., Goddéris, Y., Gerya, T. V., & Pellissier, L. (2024). Biogeographic climate sensitivity controls Earth system response to large igneous province carbon degassing. Science, 385(6709), 661-666. https://doi.org/10.1126/science.adn3450

Rohling, E. J., Marino, G., Foster, G. L., Goodwin, P. A., Von der Heydt, A. S., & Köhler, P. (2018). Comparing climate sensitivity, past and present. Annual Review of Marine Science, 10(1), 261-288. https://doi.org/10.1146/annurev-marine-121916-063242

Romps, D. M., Seeley, J. T., & Edman, J. P. (2022). Why the forcing from carbon dioxide scales as the logarithm of its concentration. Journal of Climate, 35(13), 4027-4047. https://doi.org/10.1175/JCLI-D-21-0275.1

Schmidt, A., Leadbetter, S., Theys, N., Carboni, E., Witham, C. S., Stevenson, J. A., et al. (2015). Satellite detection, long-range transport, and air quality impacts of volcanic sulfur dioxide from the 2014-2015 flood lava eruption at Bárðarbunga (Iceland). Journal of Geophysical Research: Atmospheres, 120(18), 9739-9757. https://doi.org/10.1002/2015JD023638

Schmidt, A., Skeffington, R. A., Thordarson, T., Self, S., Forster, P. M., Rap, A., et al. (2016). Selective environmental stress from sulphur emitted by continental flood basalt eruptions. Nature Geoscience, 9(1), 77-82. https://doi.org/10.1038/ngeo2588

Self, S., Schmidt, A., & Mather, T. (2014). Emplacement characteristics, time scales, and volcanic gas release rates of continental flood basalt eruptions on Earth. Geological Society of America Special Papers, 505, 319-337. https://doi.org/10.1130/2014.2505(16)

Self, S., Zhao, J.-X., Holasek, R. E., Torres, R. C., & King, A. J. (1993). The atmospheric impact of the 1991 Mount Pinatubo eruption.

Self, S., Schmidt, A., & Mather, T. (2014). Emplacement characteristics, time scales, and volcanic gas release rates of continental flood basalt eruptions on Earth. Geological Society of America Special Papers, 505, 319-337. https://doi.org/10.1130/2014.2505(16)

Self, S., Mittal, T., & Jay, A. E. (2021). Thickness characteristics of pāhoehoe lavas in the Deccan Province, Western Ghats, India, and in continental flood basalt provinces elsewhere. Frontiers in Earth Science, 8, 630604. https://doi.org/10.3389/feart.2020.630604

1062 Self, S., Mittal, T., Dole, G., & Vanderkluysen, L. (2022). Toward Understanding Deccan
1063 Volcanism. Annual Review of Earth and Planetary Sciences, 50, 477-506.
1064 https://doi.org/10.1146/annurev-earth-012721-051416
1065
1066 Sprain, C. J., Renne, P. R., Vanderkluysen, L., Pande, K., Self, S., & Mittal, T. (2019). The eruptive
1067 tempo of Deccan volcanism in relation to the Cretaceous-Paleogene boundary. Science,
1068 363(6429), 866-870. https://doi.org/10.1126/science.aav1446
1069
1070 Sulpis, O., Boudreau, B. P., Mucci, A., Jenkins, C., Trossman, D. S., Arbic, B. K., & Key, R. M.
1071 (2018). Current $CaCO_3$ dissolution at the seafloor caused by anthropogenic CO_2. Proceedings of
1072 the National Academy of Sciences, 115(46), 11700-11705.
1073 https://doi.org/10.1073/pnas.1804250115
1074
1075 Tosca, N. J., & Tutolo, B. M. (2023). Alkalinity in theory and practice. Elements, 19(1), 7-9.
1076 https://doi.org/10.2138/gselements.19.1.7
1077
1078 Wang, X., Randel, W., Zhu, Y., Tilmes, S., Starr, J., Yu, W., et al. (2023). Stratospheric climate
1079 anomalies and ozone loss caused by the Hunga Tonga-Hunga Ha'apai volcanic eruption. Journal
1080 of Geophysical Research: Atmospheres, 128(22), e2023JD039480.
1081 https://doi.org/10.1029/2023JD039480
1082
1083 White, R. V., & Saunders, A. D. (2005). Volcanism, impact and mass extinctions: incredible or
1084 credible coincidences? Lithos, 79(3-4), 299-316. https://doi.org/10.1016/j.lithos.2004.09.016
1085
1086 Wignall, P. B. (2001). Large igneous provinces and mass extinctions. Earth-Science Reviews,
1087 53(1-2), 1-33. https://doi.org/10.1016/S0012-8252(00)00037-4
1088

Wood, M., Hayes, C. T., & Paytan, A. (2022). Global Quaternary Carbonate Burial: Proxy-and Model-Based Reconstructions and Persisting Uncertainties. Annual Review of Marine Science, 15. https://doi.org/10.1146/annurev-marine-031122-031137

Xu, Y.-Y., Pierrot, D., & Cai, W.-J. (2017). Ocean carbonate system computation for anoxic waters using an updated CO2SYS program. Marine Chemistry, 195, 90-93. https://doi.org/10.1016/j.marchem.2017.07.002

Zeebe, R. E. (2011). On the molecular diffusion coefficients of dissolved CO_2, HCO_3^-, and CO_3^{2-} and their dependence on isotopic mass. Geochimica et Cosmochimica Acta, 75(9), 2483-2498. https://doi.org/10.1016/j.gca.2011.02.010

Zeebe, R. E. (2012). LOSCAR: Long-term ocean-atmosphere-sediment carbon cycle reservoir model v2. 0.4. Geoscientific Model Development, 5(1), 149. https://doi.org/10.5194/gmd-5-149-2012

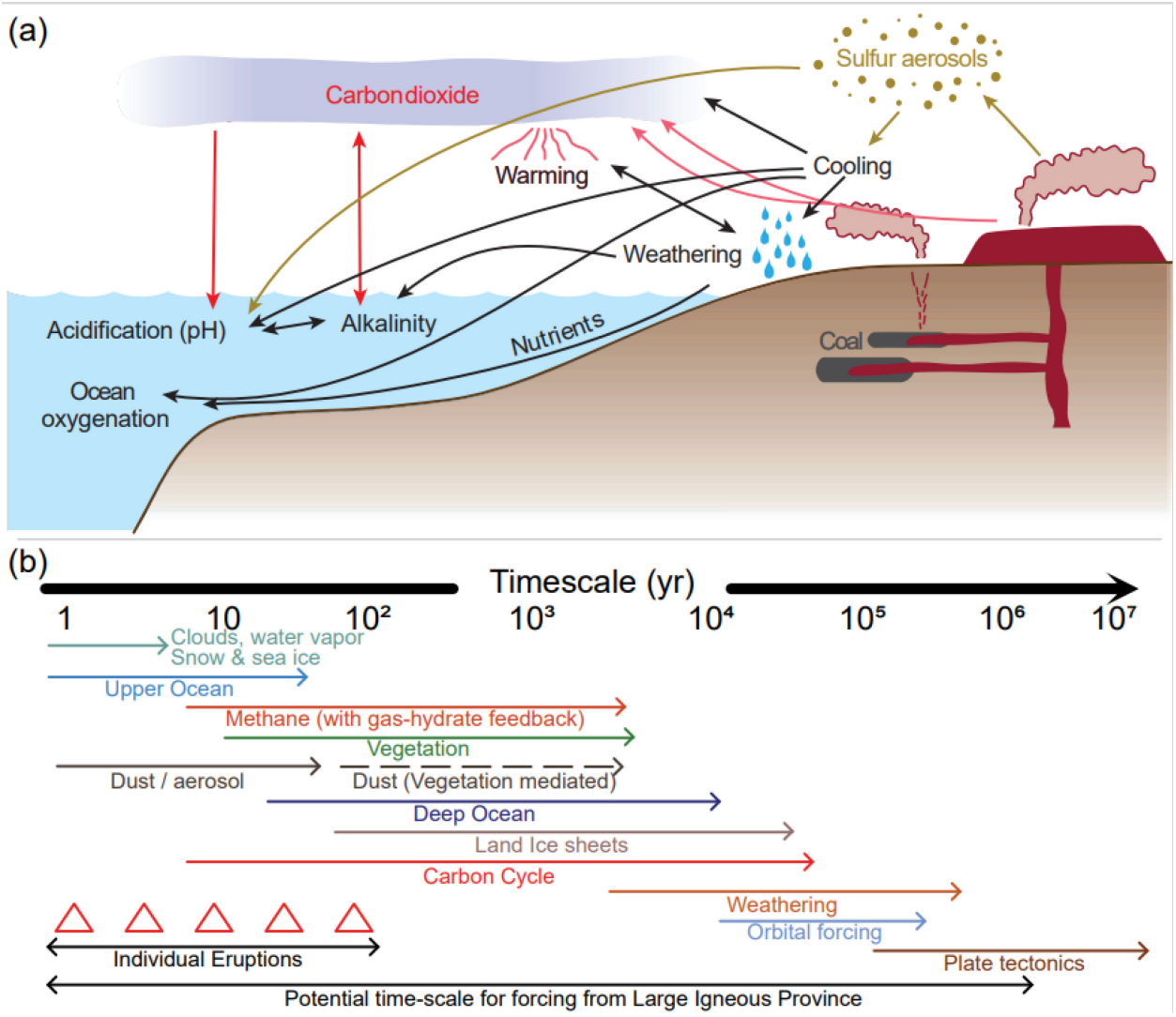
(a)
Carbondioxide
Sulfur aerosols
Warming
Cooling
Weathering
Acidification (pH)
Alkalinity
Nutrients
Ocean
oxygenation
Coal
(b)
Timescale (yr)
1
10
10²
10³
10⁴
10⁵
10⁶
10⁷
Clouds, water vapor
Snow & sea ice
Upper Ocean
Methane (with gas-hydrate feedback)
Vegetation
Dust / aerosol
Dust (Vegetation mediated)
Deep Ocean
Land Ice sheets
Carbon Cycle
Weathering
Orbital forcing
Plate tectonics
Individual Eruptions
Potential time-scale for forcing from Large Igneous Province

Figure 1.

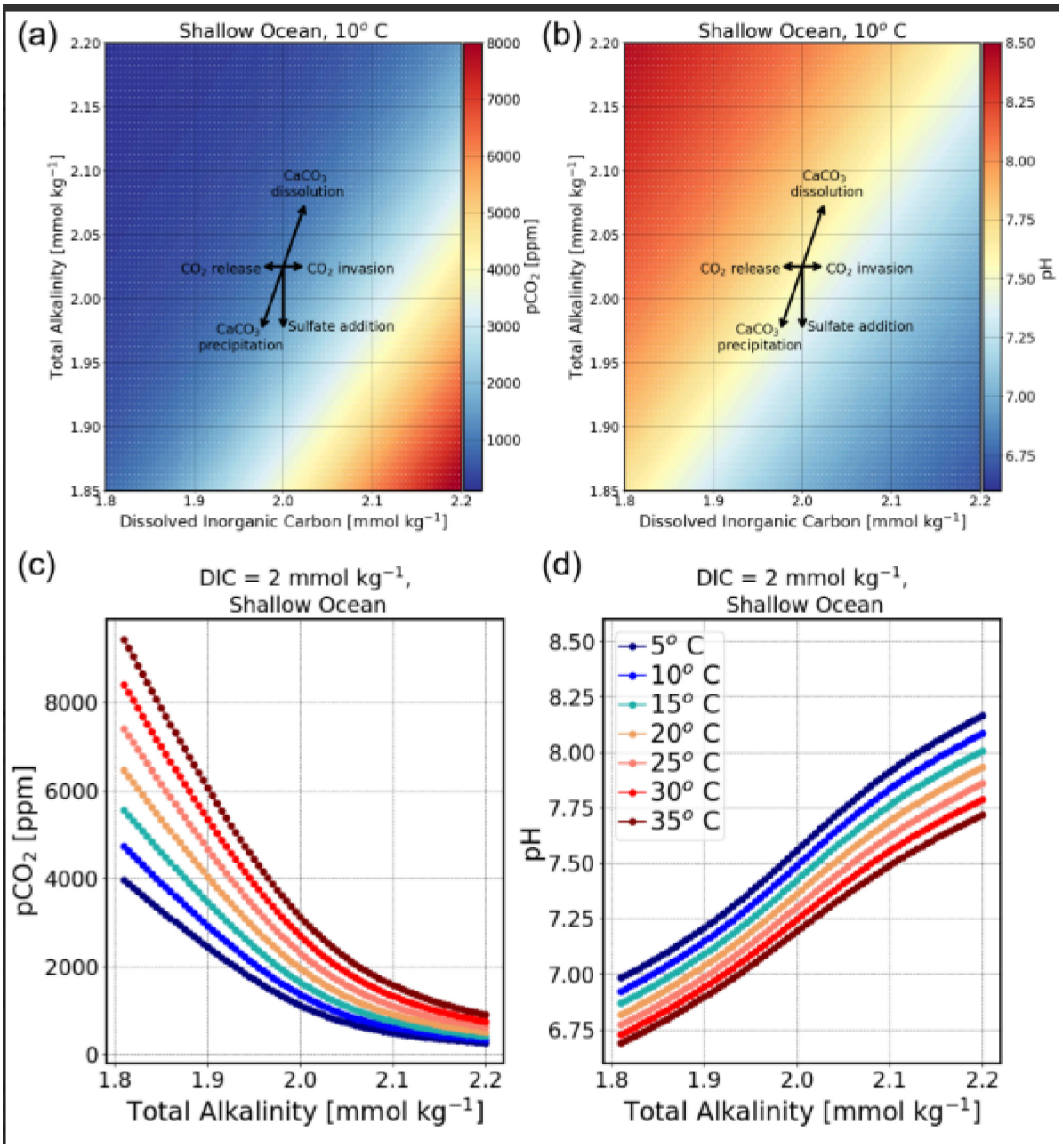
(a)
Shallow Ocean, 10° C
Total Alkalinity [mmol kg⁻¹]
Dissolved Inorganic Carbon [mmol kg⁻¹]
pCO₂ [ppm]
CaCO₃ dissolution
CO₂ release
CO₂ invasion
CaCO₃ precipitation
Sulfate addition
(b)
Shallow Ocean, 10° C
pH
(c)
DIC = 2 mmol kg⁻¹, Shallow Ocean
(d)
DIC = 2 mmol kg⁻¹, Shallow Ocean
5° C
10° C
15° C
20° C
25° C
30° C
35° C

Figure 2.

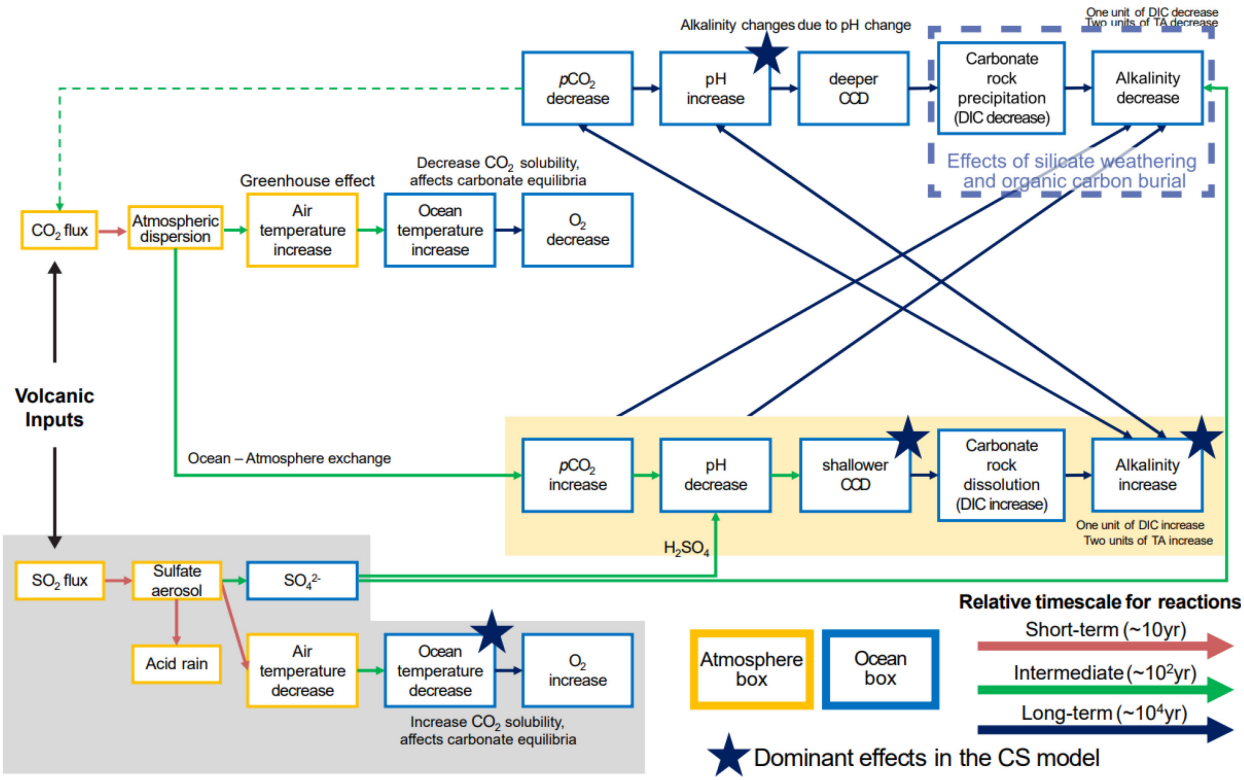
Alkalinity changes due to pH change
One unit of DIC decrease
Two units of TA decrease
pCO_2 decrease
pH increase
deeper CCD
Carbonate rock precipitation (DIC decrease)
Alkalinity decrease
Effects of silicate weathering and organic carbon burial
Greenhouse effect
Decrease CO_2 solubility, affects carbonate equilibria
CO_2 flux
Atmospheric dispersion
Air temperature increase
Ocean temperature increase
O_2 decrease
Volcanic Inputs
Ocean – Atmosphere exchange
pCO_2 increase
pH decrease
shallower CCD
Carbonate rock dissolution (DIC increase)
Alkalinity increase
One unit of DIC increase
Two units of TA increase
H_2SO_4
SO_2 flux
Sulfate aerosol
SO_4^{2-}
Acid rain
Air temperature decrease
Ocean temperature decrease
O_2 increase
Increase CO_2 solubility, affects carbonate equilibria
Relative timescale for reactions
Short-term (~10yr)
Intermediate (~10^2yr)
Long-term (~10^4yr)
Atmosphere box
Ocean box
Dominant effects in the CS model

Figure 3.

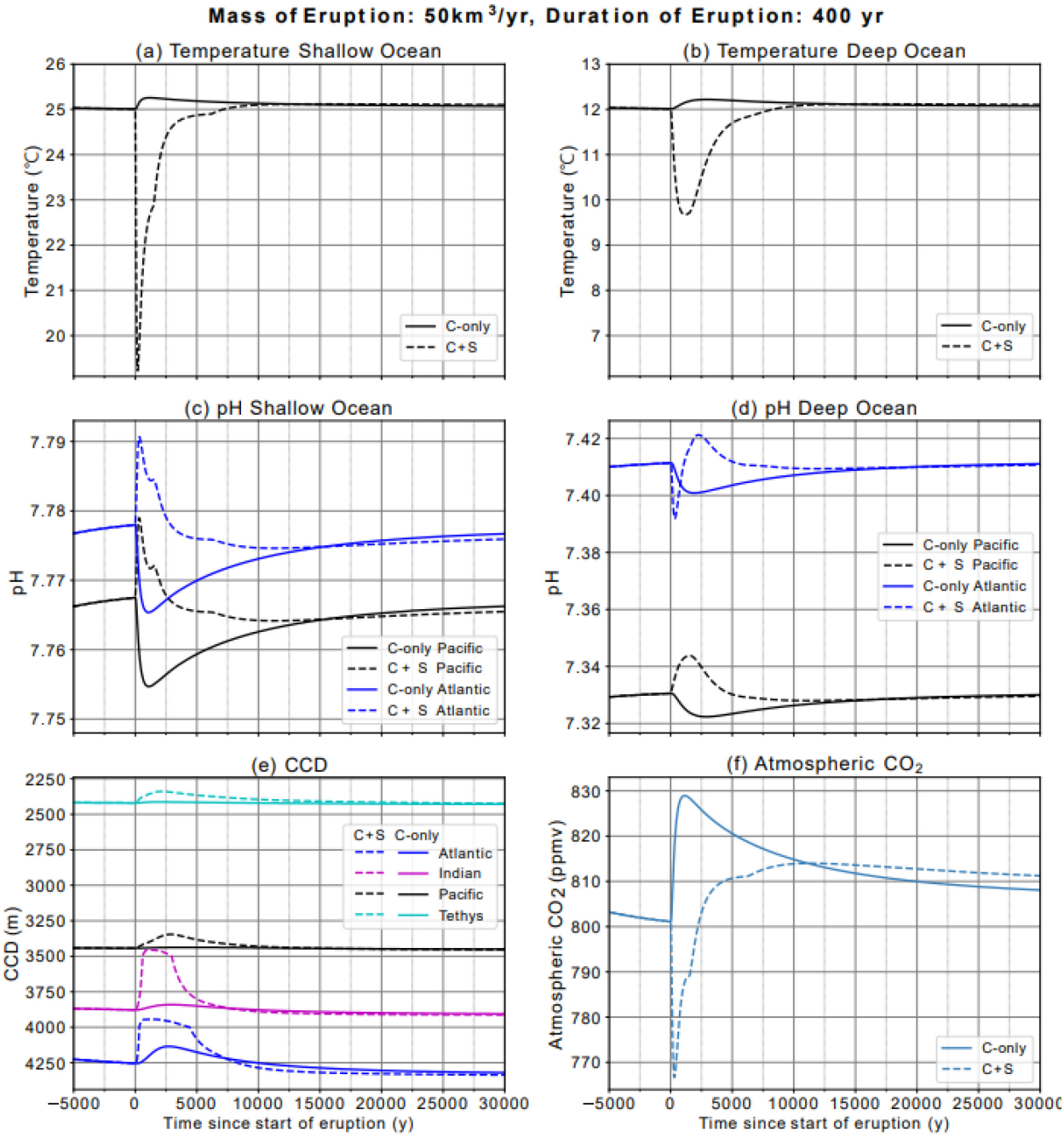
Mass of Eruption: 50km³/yr, Duration of Eruption: 400 yr
(a) Temperature Shallow Ocean
Temperature (℃)
C-only
C+S
(b) Temperature Deep Ocean
Temperature (℃)
C-only
C+S
(c) pH Shallow Ocean
pH
C-only Pacific
C + S Pacific
C-only Atlantic
C + S Atlantic
(d) pH Deep Ocean
pH
C-only Pacific
C + S Pacific
C-only Atlantic
C + S Atlantic
(e) CCD
CCD (m)
C+S C-only
Atlantic
Indian
Pacific
Tethys
Time since start of eruption (y)
(f) Atmospheric CO2
Atmospheric CO2 (ppmv)
C-only
C+S
Time since start of eruption (y)

Figure 4.

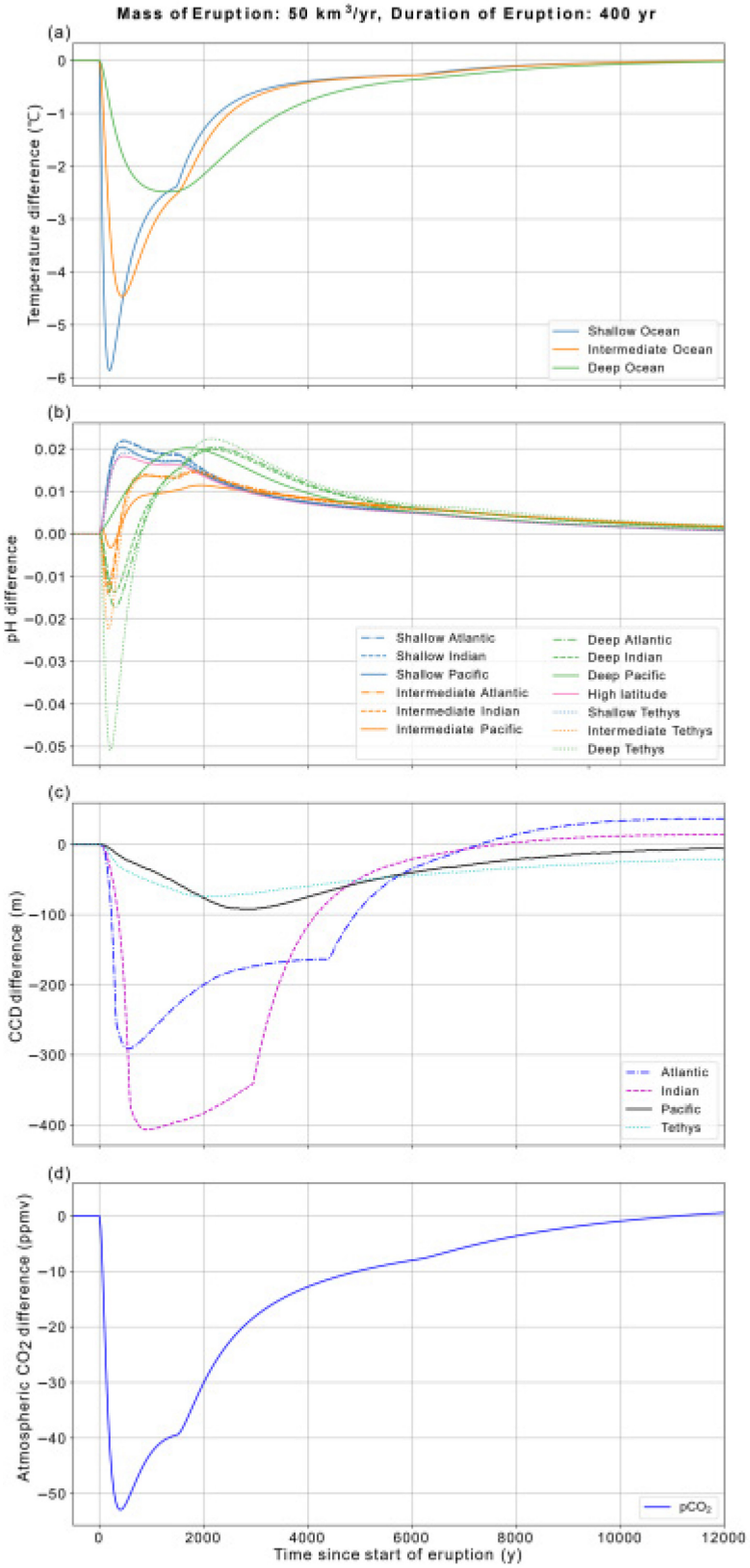
Mass of Eruption: 50 km³/yr, Duration of Eruption: 400 yr
(a)
Temperature difference (°C)
Shallow Ocean
Intermediate Ocean
Deep Ocean
(b)
pH difference
Shallow Atlantic
Shallow Indian
Shallow Pacific
Intermediate Atlantic
Intermediate Indian
Intermediate Pacific
Deep Atlantic
Deep Indian
Deep Pacific
High latitude
Shallow Tethys
Intermediate Tethys
Deep Tethys
(c)
CCD difference (m)
Atlantic
Indian
Pacific
Tethys
(d)
Atmospheric CO2 difference (ppmv)
pCO2
Time since start of eruption (y)

Figure 5.

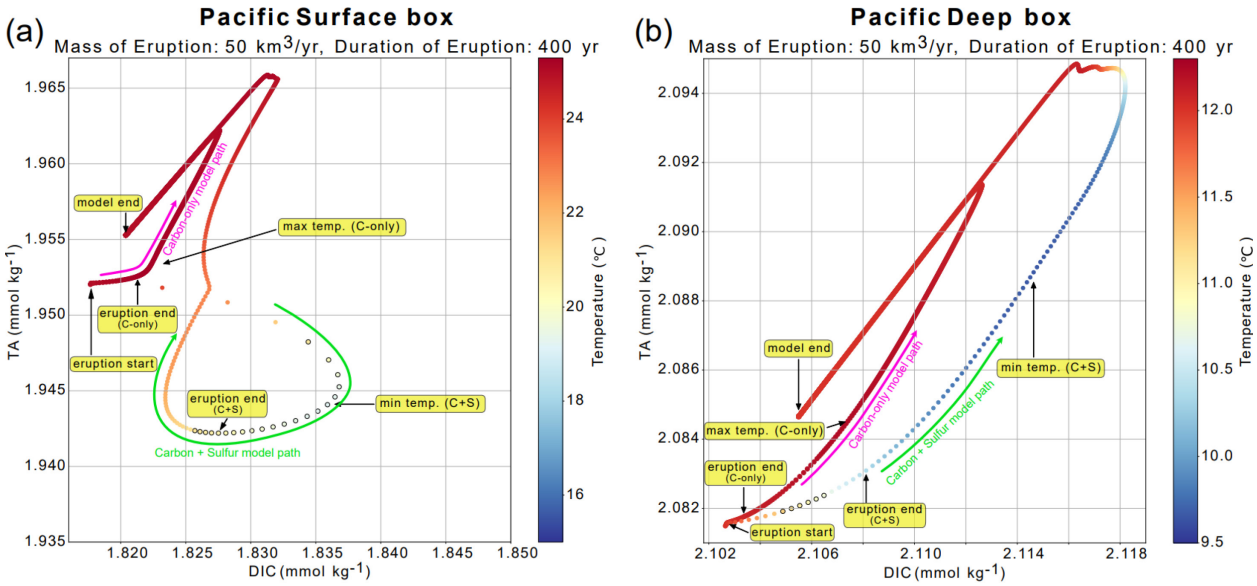
(a)
Pacific Surface box
Mass of Eruption: 50 km3/yr, Duration of Eruption: 400 yr
model end
Carbon-only model path
max temp. (C-only)
eruption end (C-only)
eruption start
eruption end (C+S)
min temp. (C+S)
Carbon + Sulfur model path
TA (mmol kg-1)
DIC (mmol kg-1)
Temperature (°C)
(b)
Pacific Deep box
Mass of Eruption: 50 km3/yr, Duration of Eruption: 400 yr
model end
max temp. (C-only)
Carbon-only model path
min temp. (C+S)
Carbon + Sulfur model path
eruption end (C-only)
eruption end (C+S)
eruption start
TA (mmol kg-1)
DIC (mmol kg-1)
Temperature (°C)

Figure 6.

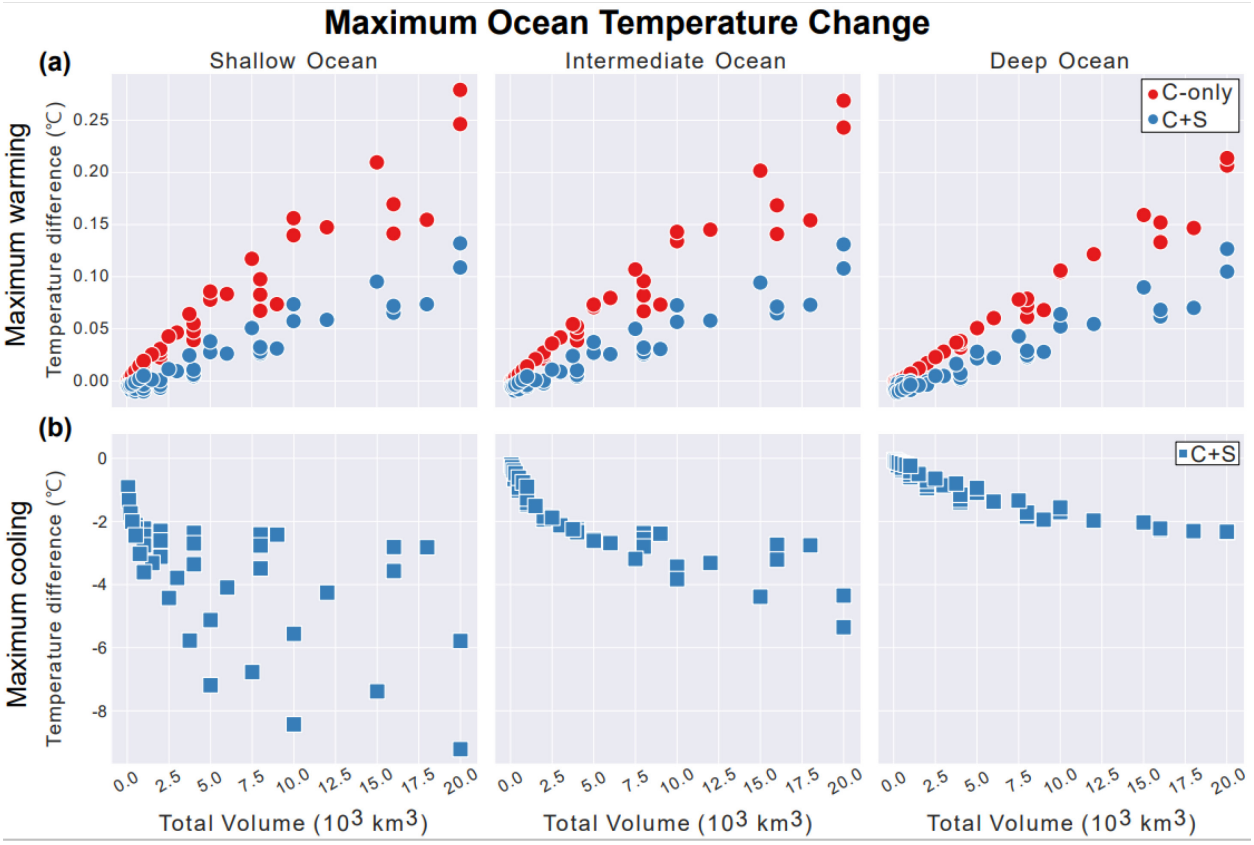
Maximum Ocean Temperature Change
(a)
Shallow Ocean
Intermediate Ocean
Deep Ocean
C-only
C+S
Maximum warming
Temperature difference (℃)
0.25
0.20
0.15
0.10
0.05
0.00
(b)
C+S
Maximum cooling
Temperature difference (℃)
0
-2
-4
-6
-8
0.0
2.5
5.0
7.5
10.0
12.5
15.0
17.5
20.0
Total Volume (10³ km³)

Figure 7.

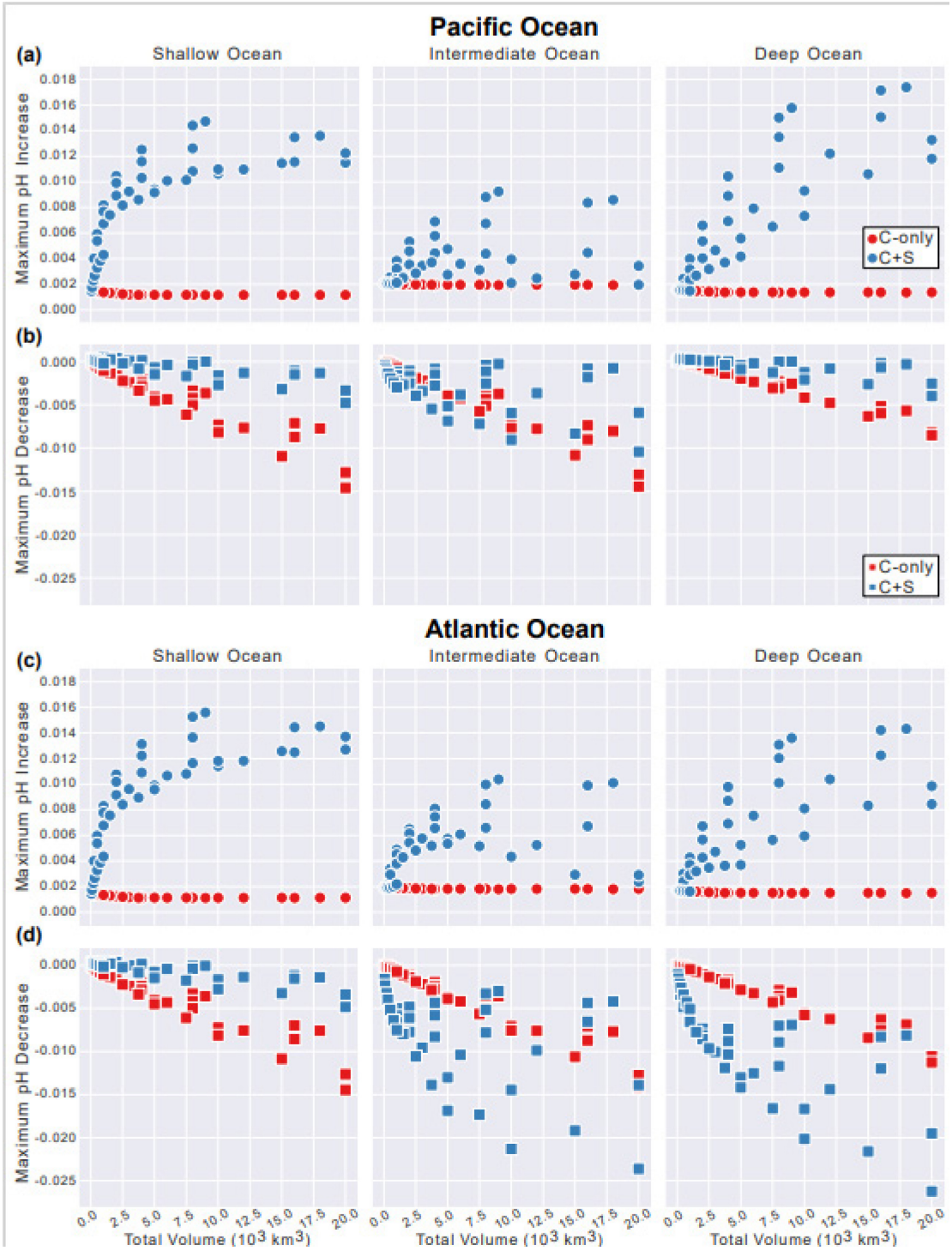
Pacific Ocean
(a)
Shallow Ocean
Intermediate Ocean
Deep Ocean
Maximum pH Increase
0.018
0.016
0.014
0.012
0.010
0.008
0.006
0.004
0.002
0.000
C-only
C+S
(b)
Maximum pH Decrease
0.000
-0.005
-0.010
-0.015
-0.020
-0.025
C-only
C+S
Atlantic Ocean
(c)
Shallow Ocean
Intermediate Ocean
Deep Ocean
Maximum pH Increase
(d)
Maximum pH Decrease
0.0
2.5
5.0
7.5
10.0
12.5
15.0
17.5
20.0
Total Volume (10^3 km^3)

Figure 8.